5. Physical Volcanology of Volcanogenic Massive Sulfide Deposits

By Lisa A. Morgan and Klaus J. Schulz

5 of 21

Volcanogenic Massive Sulfide Occurrence Model

Scientific Investigations Report 2010–5070–C

U.S. Department of the Interior
U.S. Geological Survey

U.S. Department of the Interior
KEN SALAZAR, Secretary

U.S. Geological Survey
Marcia K. McNutt, Director

U.S. Geological Survey, Reston, Virginia: 2012

Suggested citation:
Morgan, L.A., and Schulz, K.J., 2012, Physical volcanology of volcanogenic massive sulfide deposits in volcanogenic massive sulfide occurrence model: U.S. Geological Survey Scientific Investigations Report 2010–5070 –C, chap. 5, 36 p.

Contents

Figures

Tables

5. Physical Volcanology of Volcanogenic Massive Sulfide Deposits

By Lisa A. Morgan and Klaus J. Schulz

Introduction

Volcanogenic massive sulfide (VMS) deposits form at or near the seafloor in a variety of marine volcano-tectonic terranes (fig. 5–1). These deposits form from a spectrum of volcanic and hydrothermal processes (fig. 5–2), include a broad range of chemical compositions, occur in a variety of tectonic settings, and commonly display marked contrasts in physical characteristics between the ore body and its host rock. Volcanogenic massive sulfide deposits are enriched in Cu, Pb, Zn, Au, and Ag and are significant global sources of these elements. Approximately 1,100 VMS deposits have been identified worldwide with a total estimated resource of about 10 Bt (billion tons) (Mosier and others, 2009).

A highly effective approach in understanding the origin and evolution of VMS deposits is the application of physical volcanology, the study of eruption dynamics and emplacement processes responsible for the resultant deposit(s). Physical volcanology is especially useful in hydrothermally altered and metamorphosed volcanic terranes. In general, physical volcanology is used (1) to identify the products and deposits associated with volcanic eruptions; (2) to understand the complex mechanisms associated with eruptions; (3) to comprehend mechanisms of emplacement and post-emplacement processes of the deposits; and (4) to recognize volcanic terranes by their geomorphology (Gibson and others, 1999; Gibson, 2005).

Physical volcanology is important in the classification of VMS deposits (McPhie and others, 1993; Gibson and others, 1999) (fig. 5–2). The controls on whether an eruption is explosive or effusive include the magma composition, volatile content, eruption rate, viscosity, and ambient conditions, especially the presence of external water and ambient pressure (Cas and Wright, 1987; Cas, 1992). The reconstruction of volcanic history through facies analyses and stratigraphic correlation permits the paleogeographic and geotectonic environment of older volcanic terranes to be revealed. This provides a framework to understand the controls for localization of mineralization. Recognition of distinctive volcanic facies and facies associations is critical to reconstructing the original facies architecture of the system (McPhie and Allen, 1992). Techniques such as geologic mapping, stratigraphic and facies analyses, geochemical and geophysical fingerprinting, and interpretation of core samples help define the specific volcanic-tectonic setting and contribute to the identification of distinct volcanic environments that are favorable for the formation of VMS deposits. This approach enhances predictive capability and provides a basis for establishing criteria for exploration.

We use the classification system of Franklin and others (2005) and Galley and others (2007), recognizing five lithostratigraphic deposit types and associated tectonic terranes in which VMS deposits form (fig. 5–1). This classification scheme considers the entire stratigraphic sequence or volcano-sedimentary cycle within a district (Franklin and others, 2005). Each sequence is bounded either by faults, disconformities, or unconformities marking a significant break in the stratigraphic record (Franklin and others, 2005). Deposits within a specific district are confined to a limited volcanic episode or stratigraphic interval (Franklin, 1996), usually lasting <2 m.y. These deposits form in terranes at different levels of maturity in their evolution and include (fig. 5–1 inset):

1. primitive intraoceanic back arc, fore-arc basin, or oceanic ridge producing a mafic-ultramafic suite typified by ophiolite sequences containing <10 percent sediment (for example, Cyprus, Oman) (Franklin and others, 2005) (fig. 5–1);

2. incipient-rifted intraoceanic arcs producing a bimodal-mafic suite typified by lava flows and <25 percent felsic strata (for example, Noranda, Ural Mountains);

3. incipient-rifted continental margin arc and back arc producing a bimodal-felsic suite, typified by 35–70 percent felsic volcaniclastic strata (for example, Skellefte, Tasmania, Jerome);

4. mature epicontinental margin arc and back arc producing a siliciclastic-felsic suite dominated by continent-derived sedimentary and volcaniclastic strata (for example, Iberia, Bathurst); and

5. rifted continental margin or intracontinental rift or sedimented oceanic ridge producing a siliciclastic-mafic suite typified by subequal amounts of pelite and basalt (for example, Windy Craggy, Besshi).

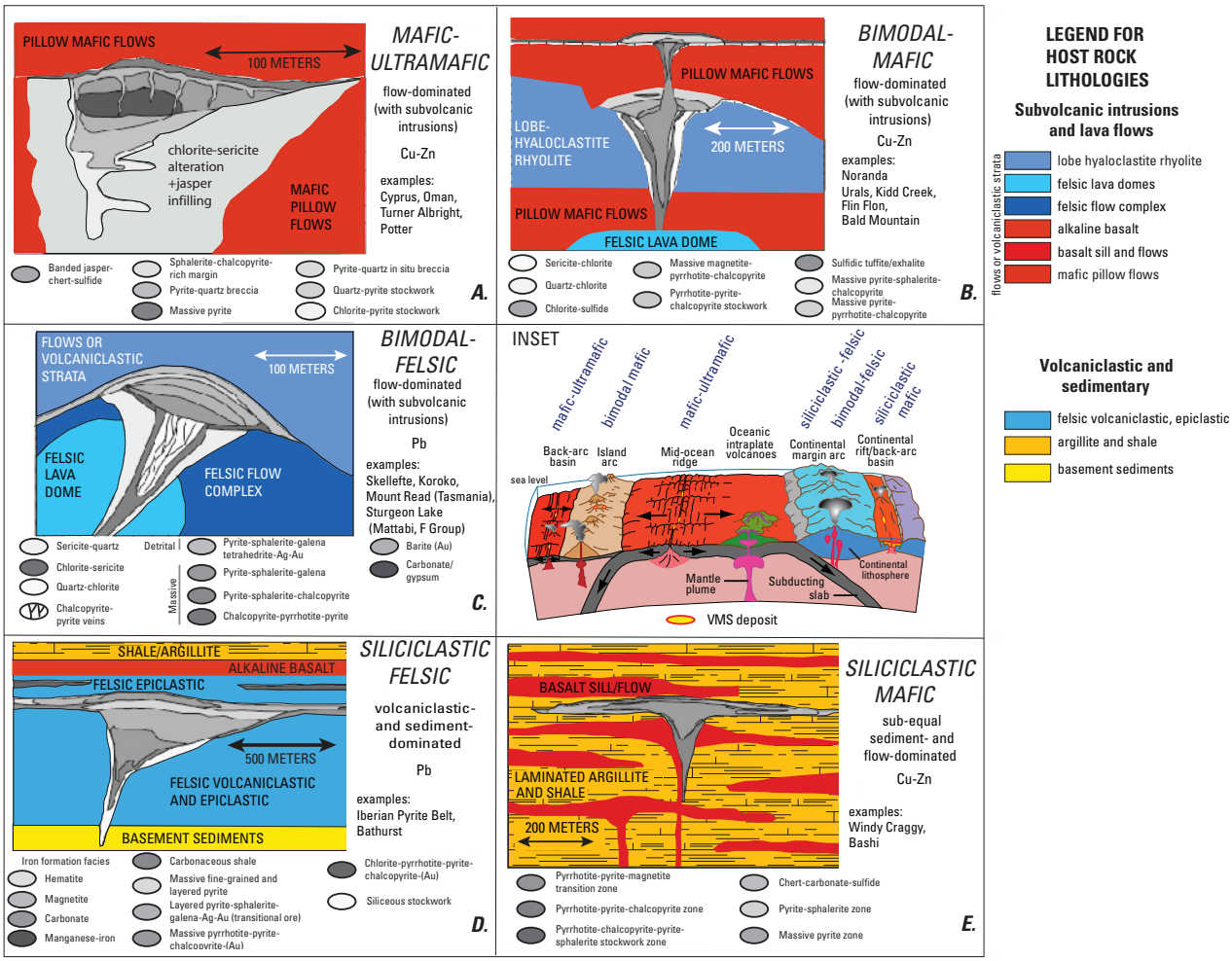

Figure 5–1. Graphic representations of the lithological classification used in this study (modified from Barrie and Hannington, 1999, by Franklin and others, 2005). Emphasized here in color (red generally for mafic compositions, blue generally for felsic compositions) are the volcanic, volcaniclastic, or sediment host rocks for each lithofacies unit; examples of associated VMS deposits are represented in shades of gray and are listed. The inset (from fig. 4-2, this volume) identifies the tectonic environment for each volcanic terrane; the individual type of associated lithofacies is shown as larger italicized letters above their respective terranes. Modified from Galley and others (2005). [Ag, silver; Au, gold; Cu, copper; Pb, lead; Zn, zinc]

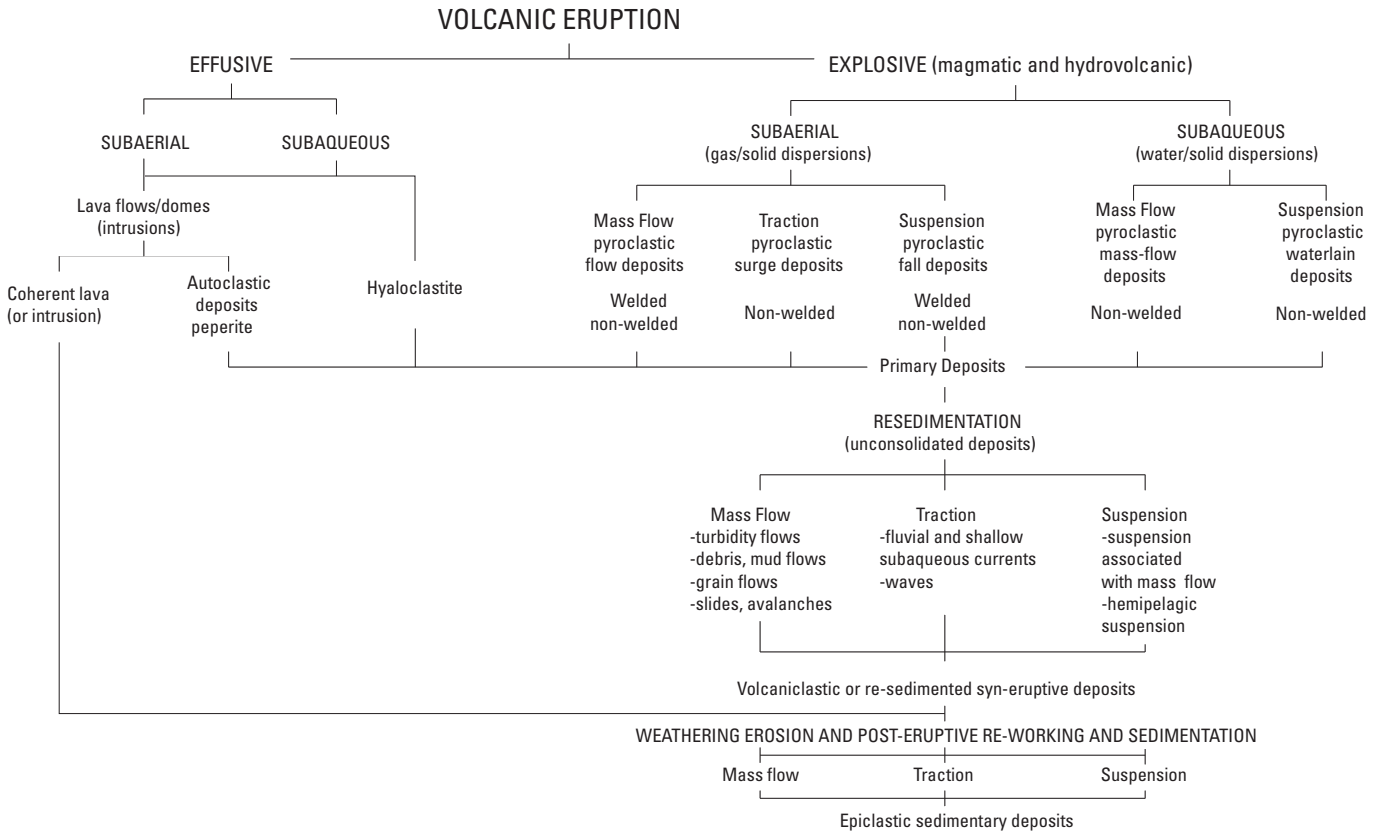

Figure 5–2. Genetic classification of volcanic deposits erupted in water and air (from Gibson and others, 1999).

The mafic-ultramafic, bimodal-mafic, and siliciclastic-mafic volcanic suites are associated with ocean-ocean subduction-related processes and represent various stages in the evolution of arc development (Franklin and others, 2005). Bimodal-felsic and siliciclastic-felsic volcanic suites are associated with continental margins to back-arc environments. These suites were developed in submarine environments where about 85 percent of all volcanism on Earth occurs (White and others, 2003). Tables 5–1 and 5–2 consider the differences for subaerial volcanic deposits versus those emplaced in subaqueous environments, prime locales for VMS deposition.

Volcanogenic massive sulfide mineralization occurs in two main types of volcanic deposit associations, each of which may contain subordinate sedimentary lithofacies: lava flow–dominated lithofacies associations and volcaniclastic-dominated lithofacies associations. These associations are suggested to correspond in general to deposits that formed in deep water versus shallow water volcanic environments, respectively (Gibson and others, 1999) (fig. 5–3*A*). A third lithofacies type that hosts or is associated with VMS mineralization is sediment dominated (see fig. 4–8).

Volcanic processes and deposits have a major influence on modifying their physical environments (for example, water depth, elevation, gradient, and relief) (McPhie and Allen, 1992) (fig. 5–3). Explosive volcanism can occur suddenly and can erupt large volumes of pyroclastic material resulting in abnormal sedimentation rates, changes in drainage patterns, and deposition of lateral facies that represent contrasting emplacement processes. Of all rock types, volcanic rocks have the largest range of physical properties, including density, porosity, permeability, and chemical stability. Post-emplacement processes such as vitrification, devitrification, quenching, welding, degassing, and alteration impose additional variability in the diversity and properties of rock types. Volcanic rocks can be emplaced at extremely high and low temperatures and in dry and wet forms. Discharge rate and magma composition control the shapes and dimensions of lava flows (Walker, 1992).

The bulk density of overlying host strata and the density of magmas that intrude the sequence influence the type of volcanism and whether lavas are emplaced on the surface, intrude into wet sediment and mix to create peperite, intrude into the sediments as invasive flows, or are emplaced as shallow dikes and sills never reaching the surface. Multiple and overlapping volcanic events may be contemporaneous but not genetically related (fig. 5–4), and thus it is critical in establishing the volcanic history of the terrane that the different volcanic environments responsible for emplacement of specific volcanic deposits are understood and can be identified (McPhie and Allen, 1992; McPhie and others, 1993).

Table 5–1. Comparison of some important properties of air versus water and their effects on eruptions. Note the similar values for the viscosity of steam and the values for heat capacity to those of air. Heat capacity per volume for both air and steam is much lower than that of water; the values in the table are heat capacity per kilogram. Thermal conductivity of water is about 20 times that of air, but steam has a thermal conductivity almost 50 times that of water.

[Source: White, 2003. kg/m^3, kilogram per cubic meters; mPa•s, millipascal-second; J/kg•K, joule per kilogram-Kelvin; W/m•K, watt per meter-Kelvin; °C, degree Celcius; K, Kelvin; STP, standard conditions for temperature and pressure]

Air	Water (*steam)
Density	
1.239 kg/m^3 (cold dry air at sea level) decreases with altitude	1,000 kg/m^3 (fresh water, standard conditions)
	1,025 kg/m^3 (typical surface seawater)
Viscosity	
0.0179 mPa•s (millipascal) at 15°C, STP	1.00 mPa•s (millipascal) at 20°C, STP
	* 0.01 mPa•s (millipascal) saturated steam, STP
Specific heat capacity	
1,158 J/kg•K (at 300 K)	4,148.8 J/kg•K (liquid water at 20°C)
	* 1,039.2 J/kg•K (water vapor at 100°C)
Thermal conductivity	
0.025 W/m•K (air at sea level)	0.56 W/m•K (liquid water at 273 K)
	* 27.0 (water vapor at 400 K)
	** 2.8 (ice at 223 K)

Role of Water in Submarine Volcanism

Water plays an important role in controlling and influencing the physical nature of volcanism. Over two thirds of the Earth's surface is below sea level and, as recent submarine investigations reveal, volcanism is more common on the seafloor than in the subaerial environment (Fisher and others, 1997). Until recently, few eruptions on the seafloor have been witnessed, but those that have been witnessed on the seafloor (Chadwick and others, 2008) have provided new and insightful observations (Kessel and Busby, 2003; Cashman and others, 2009; Chadwick and others, 2009). Much remains to be learned about the effects of ambient water and hydrostatic pressure on volcanic eruptions in deep marine environments (fig. 5–2; tables 5–1, 5–2) (see also Busby, 2005; Clague and others, 2009).

The environment of formation for all VMS deposits is subaqueous and, thus, water strongly influences subsequent volcanic processes and the physical nature of rock created. Water creates a very different set of conditions for submarine volcanism compared to more frequently observed subaerial volcanism. In the submarine environment, ambient temperatures may be at near-freezing temperatures; pressures can range up to 500 bars (approximately 5000 m water depth) or more (McBirney, 1963). Water can be locally heated by lava and change rapidly from a liquid phase to a vapor phase, resulting in a sudden increase in total volume.

Classification System

Figure 5–1 highlights the volcanic and sedimentary rock types for each major VMS deposit subtype in the classification system used. The volcanic deposits can be subdivided and grouped into two primary environments: (1) those dominated by high-level dikes, sills, cryptodomes, and lava flows (fig. 5–1-A, B, C), and (2) those dominated by volcaniclastic and sedimentary sequences (fig. 5D, E). The following is a summary of the physical volcanological characteristics for each of the lithostratigraphic types and associated tectonic terranes linked with VMS deposition. The focus of this chapter is on the specific terranes and specific volcanic-related deposits that are common to VMS terranes. As such, in regard to volcanic and sedimentary rocks, only those rock types that are typical to VMS deposits are discussed, including pillow basalts and other flow forms in deep water environments, lobe-hyaloclastite rhyolite, felsic lava domes, felsic flow complexes, pyroclastic deposits, flow- or volcaniclastic-dominated sequences, terrigenous clastic sediments, and shale/argillitic sequences. Subvolcanic intrusions, mapped as deep crustal bodies and plutons, provide the major sustained heat sources for VMS mineralization and are discussed at the end of this chapter.

Table 5–2. Comparison of some important environmental factors for subaqueous and subaerial eruptions.

[Source: White, 2003]

Phenomenon	Subaqueous	Effect (± trend)	Subaerial	Effect
Steam from interaction with magma, hot particles, and (or) as magmatic volatile	Ubiquitously formed above critical depths by interaction of magma with ambient water, films on hot clasts, from magma at shallower than critical depths	Expansion (may be violent), high buoyancy, low heat capacity compared to water, steam formation suppressed with depth; disappears at ~3 km in seawater	Steam from interaction with magma only in "wet " sites, steam in eruption plume also from heating of air entrained, and from magma	Expansion (may be violent), buoyant when hot, condensing water alters particle transport properties (for example, adhesion) heat capacity similar to air
Pressure	Hydrostatic pressure	Damps expansion of steam from boiling and of magmatic gases; in combination with cooling, condenses gas in eruption plumes to produce aqueous plumes or currents; effect increases strongly with depth	Atmospheric pressure	Allows expansion of gases; eruption plumes are at maximum pressure near vent exit, and pressure decreases gradually with height in atmosphere
Thermal behavior	High heat capacity	Rapid cooling of magma, hot rock (but see steam, above) can cause fragmentation by granulation	Low heat capacity	Slow cooling of magma, hot rock; granulation not effective, but dynamothermal spalling for some lavas
Rheology	High density, high viscosity	Low clast settling velocities, slower movement or expansion of plumes, currents; hot particles may be temporarily buoyant, and some pumice persistently buoyant; gas-supported currents require very high particle concentrations to remain negatively buoyant	Low density, low viscosity	High clast settling velocities, granular collisions more important in transport; all clasts more dense than atmosphere at all times; gas-supported currents negatively buoyant even at low to moderate particle concentrations

Flow Lithofacies Associations

Essential elements in the lithofacies classification include (1) coherent lava flows and domes of several compositions ranging from ultramafic to mafic to felsic; (2) possible associated autoclastic deposits (autobreccia, hyaloclastite, and redeposited equivalents) (Franklin and others, 2005); and (3) possible hosting of synvolcanic intrusions, including sills, dikes, and less commonly, cryptodomes. Minor amounts of volcaniclastic rocks are associated with some VMS deposits and range from redeposited autobreccia to primary pyroclastic deposits. Sedimentary rocks such as carbonaceous argillite, minor carbonate, immature volcaniclastic wacke, and exhalite (Franklin and others, 2005) may occur with the flow lithofacies. The flow lithofacies associations, dominated by lava flows, domes, and synvolcanic intrusions, are controlled by effusive eruptive processes. The eruptive sources for these effusive lavas and subvolcanic intrusions are commonly single or composite submarine volcanoes fed by subvolcanic dikes, sills, and cryptodomes. In some cases, VMS deposits occur in the capping caldera(s) or synvolcanic graben(s).

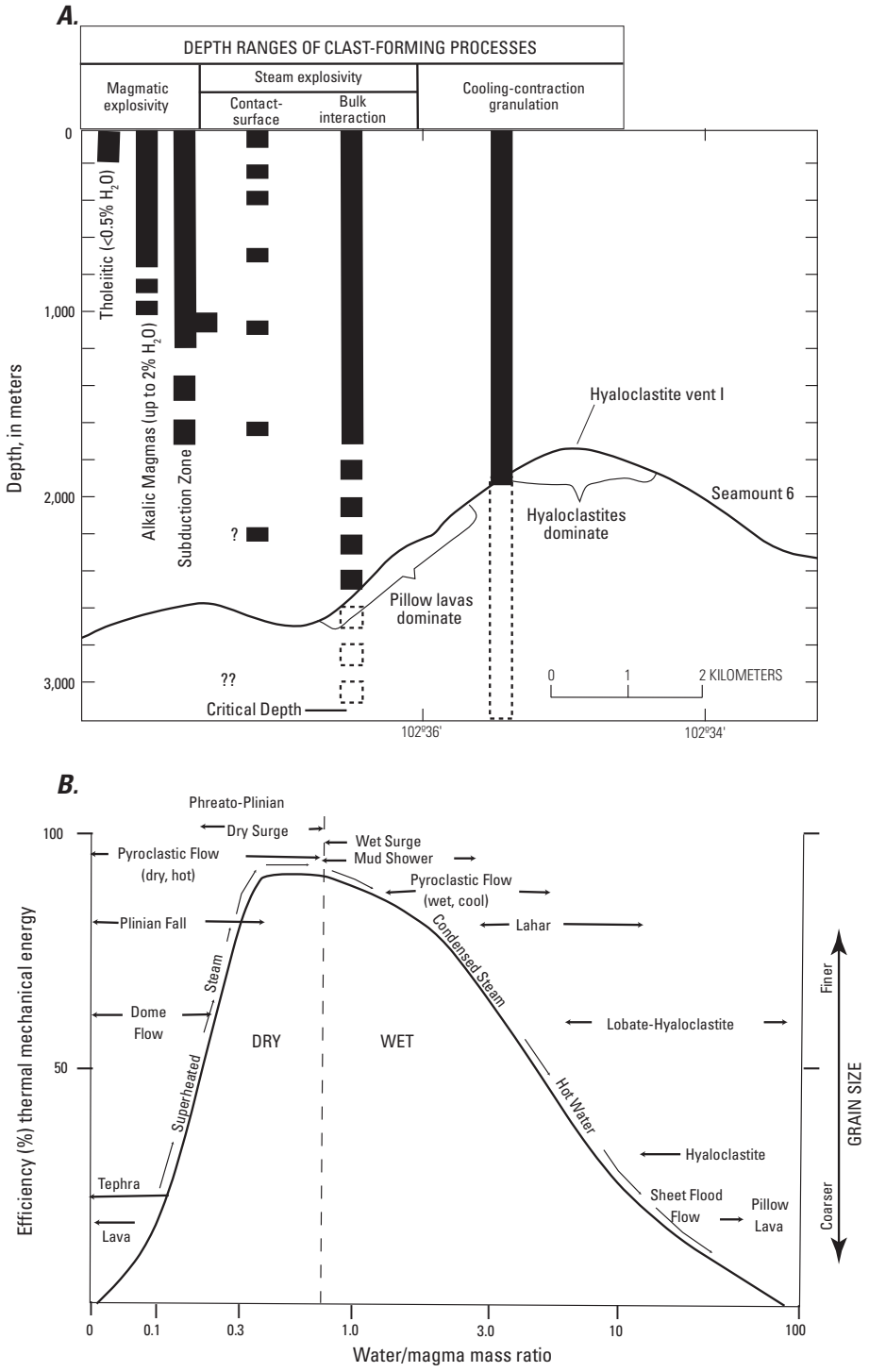

Figure 5–3. Physical conditions for volcanic eruptions. *A*, General geologic setting, conditions, and environment for magma and lava emplacement in submarine seamounts (from Head and Wilson, 2003). The cross section shown is for Seamount 6 (Eastern Pacific Ocean) but is assumed to be exemplative of conditions and observations on other seamounts (data from Smith and Batiza, 1989). Also shown are the ranges in depth of various clast-forming processes on the seafloor (from Kokelaar, 1986). *B*, Water/magma ratio versus deposit type and efficiency of fragmentation (from Gibson and others, 1999; after Wohletz and Sheridan, 1983; Wohletz, 1986; Wohletz and Heiken, 1992)

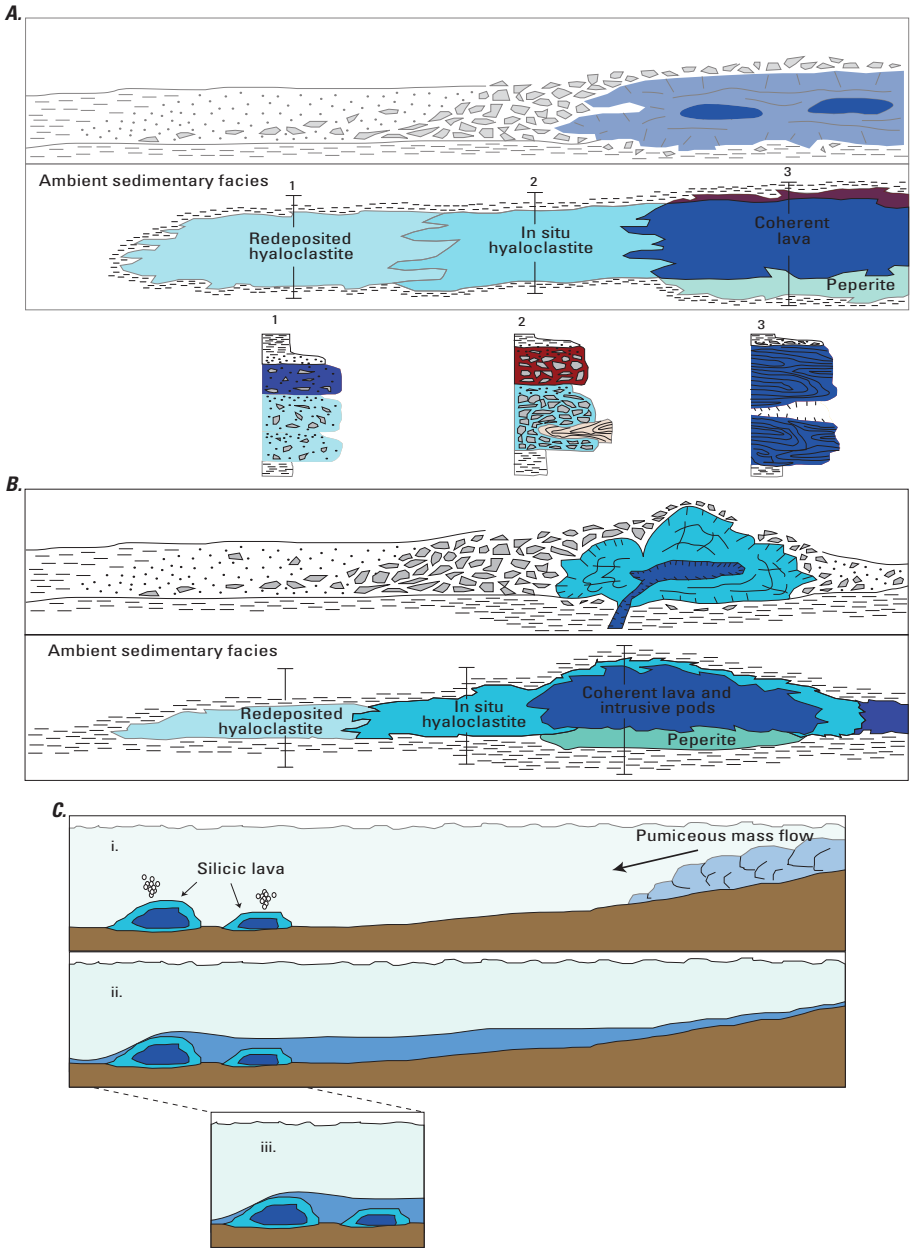

Figure 5–4. Diagrams showing different types of genetically related and nonrelated volcanic rocks and processes. *A*, Schematic cross sections through a submarine lava flow showing the character and arrangement of contemporaneous volcanic facies that develop in association with the emplacement of these lavas. Sections marked 1, 2, and 3 on the facies diagrams are defined by stratigraphic sections located between the facies diagrams. Each section shows genetically related facies that are markedly different in lithologic character, texture, and internal organization. After McPhie and others (2003). *B*, Schematic cross sections through a submarine dome showing the character and arrangement of contemporaneous volcanic facies that develop in association with the emplacement of these lavas. Sections marked 1, 2, and 3 on the facies diagrams below *A* are defined by stratigraphic sections located between the facies diagrams. Each section shows genetically related facies that are markedly different in lithologic character, texture, and internal organization. After McPhie and others (2003). *C*. Sketches illustrating penecontemporaneous, laterally equivalent volcanic facies that are not genetically related. (a) A subaqueous silicic lava dome with a brecciated carapace is emplaced and contributes considerable relief to the sea floor landscape. Pyroclastic mass flows sourced elsewhere sweep into the basin. (b) The pyroclastic mass flows are deposited as a widespread sheet and fill the topography created by the lava dome and breccia and basin. (c) The background sedimentary facies encloses the two genetically distinct volcanic facies that are directly juxtaposed and emplaced contemporaneously. From McPhie and Allen (1992).

Mafic-Ultramafic Volcanic Suite (Primitive Intraoceanic Back-Arc or Fore-Arc Basins or Oceanic Ridges)

Mafic-ultramafic suites formed during much of the Archean and Proterozoic when it is hypothesized that mantle plume activity dominated formation of Earth's early crust. Numerous incipient rifting events formed basins characterized by thick ophiolite sequences (Galley and others, 2007). A generalized stratigraphic section through an ophiolite (fig. 5–5) has (1) a series of effusive flows, mostly pillow lavas, with minimal interflow volcaniclastic material and <5 percent felsic volcanic rocks (Franklin and others, 2005) above (2) a thick section of synvolcanic intrusions in the form of sheeted dikes. These associations are typical mafic volcanic successions that form at fast ocean spreading centers or in incipient back- or fore-arc environments. This mafic succession continues downward into (3) a thick sequence of layered gabbros (representative of the crystallized magma chamber) and peridotite (representative of the depleted upper mantle beneath the magma chamber). The ultramafic suite of rocks may form in slow to ultraslow spreading environments where classic crustal successions are absent.

In deep water marine rift environments, eruptions producing pillow lava flows occur along fissures and at point sources (Cas, 1992). Such edifices include elongate shield volcanoes (fig. 5–6*A*), small isolated lava mounds, and lava lakes where the pillowed flows are ponded in fault blocks within and adjacent to the ridge axis (Gibson and others, 1999; Gibson, 2005). Such edifices have been identified as hosts to VMS deposits, such as the copper-rich ophiolite-hosted Cyprus deposits (Gibson and others, 1999) (fig. 5–1*A*).

Pillow Lava Flows in Mafic-Ultramafic Associations

Pillow lavas are among the most common volcanic rocks on Earth (Walker, 1992), having formed in underwater environments as sets of bulbous, tubular, or spherical lobes of lava fed by an interconnected system of lava tubes or channels. Pillow lavas can form in any subaqueous environment regardless of depth; they are common in deep marine environments, in glaciated environments as subglacial eruptions, and in shallow water environments such as lakes, rivers, and nearshore marine environments (Fridleifsson and others, 1982). Subaqueous development of bulbous forms by the inflation of a chilled skin that accommodates additional injections of magma is an essential attribute to pillow lava formation (Walker, 1992). Pillow lavas are produced by the rupture and subsequent piling up of individual pillow lobes; each lobe has a thick skin with a thin selvage of quenched glass (figs. 5–6*B, C, D*). Small mafic pillow lava lobes tend to be circular in cross section and flatten as their dimension increases, most likely under the influence of gravity (Cousineau and Dimroth, 1982). Each lobe has a convex upper surface and a base that is either flat or concave upward, the shape commonly being a cast of the underlying pillow form. As such, pillow lavas in basaltic and andesitic flows have a distinctive and easily identifiable morphology (Gibson and others, 1999). The size of individual pillows is a function of magma viscosity; andesite pillows are usually larger than basaltic pillows and frequently have a "breadcrusted" outer surface texture. The aspect ratio (horizontal/vertical ratio) of pillow lobes varies with andesitic lavas plotting at the upper end of the spectrum and basaltic lobes at the lower end, a relationship inferred to relate to viscosity (Walker, 1992).

A pillow lava flow is fed by an interconnected system of lava tubes or open channels that are branching and intertwined. Stratigraphic analyses of Archean submarine basalt flows often show a sequence with massive flows at the base grading upward to pillow lavas and a carapace of pillow breccias (Dimroth and others, 1978, 1985). Mapping suggests that pillows form by a budding and branching process (fig. 5–6*D*) (Moore, 1975; Dimroth and others, 1978; Walker, 1992; Goto and McPhie, 2004). Dimroth and others (1978) propose that massive lavas form by the surging advance of hot, low-viscosity lavas. Pillow lavas form at the distal end of the flow front and have lower temperatures and higher viscosities than in their massive equivalent. The decrease in temperature and increase in viscosity results in a decrease in the velocity of the flow (Walker, 1992). Most pillow mounds form not because of decrease in temperature or viscosity but because of the decrease in the supply of magma, that is, flow rate. In general, given a constant viscosity, the formation of pillow mounds is principally a function of flow rate. As the pile of pillow lobes form, fresh magma oozes through ruptures in pre-existing lobes and the pillow pile grows in this manner. Proximal pillow lavas tend to have larger pillows than distal equivalents (fig. 5–6*A*). This flow process forms steep-sided ridges or mounds that can be tens of meters thick, commonly called "haystacks." Mega-pillows, up to tens of meters in diameter, have been identified in the upper and capping parts of pillow lava flows and are interpreted to be possible master channels by which fresh lava was transported from the vent to the advancing flow front (Walker, 1992). Features, dimensions, and structures associated with pillow lobes and lavas can be used to infer flow direction and source area.

The subaerial equivalents of pillow flows are tube-fed pahoehoe lava flows. Both lava flow types are interpreted to be the products of sustained eruptions at low effusion rates. The confirmation that pillow lavas and pahoehoe lavas form by similar mechanisms came with direct observations of subaqueous lava deltas associated with eruptions into the sea from Kilauea in 1972 and 1974 (Moore, 1975). Low effusion rates allow for a thick skin to form on the exterior of lava lobes or toes and contribute to insulation of the lobe interior, allowing the interior to remain hotter and more fluid. Most pillow lava lobes are dense throughout but may contain vesicles arranged in a radial pattern in the upper sections of individual lobes due to exsolution and trapping of magmatic gases. Degassing contributes somewhat to inflation of the interior and the overall

Mafic-untramafic

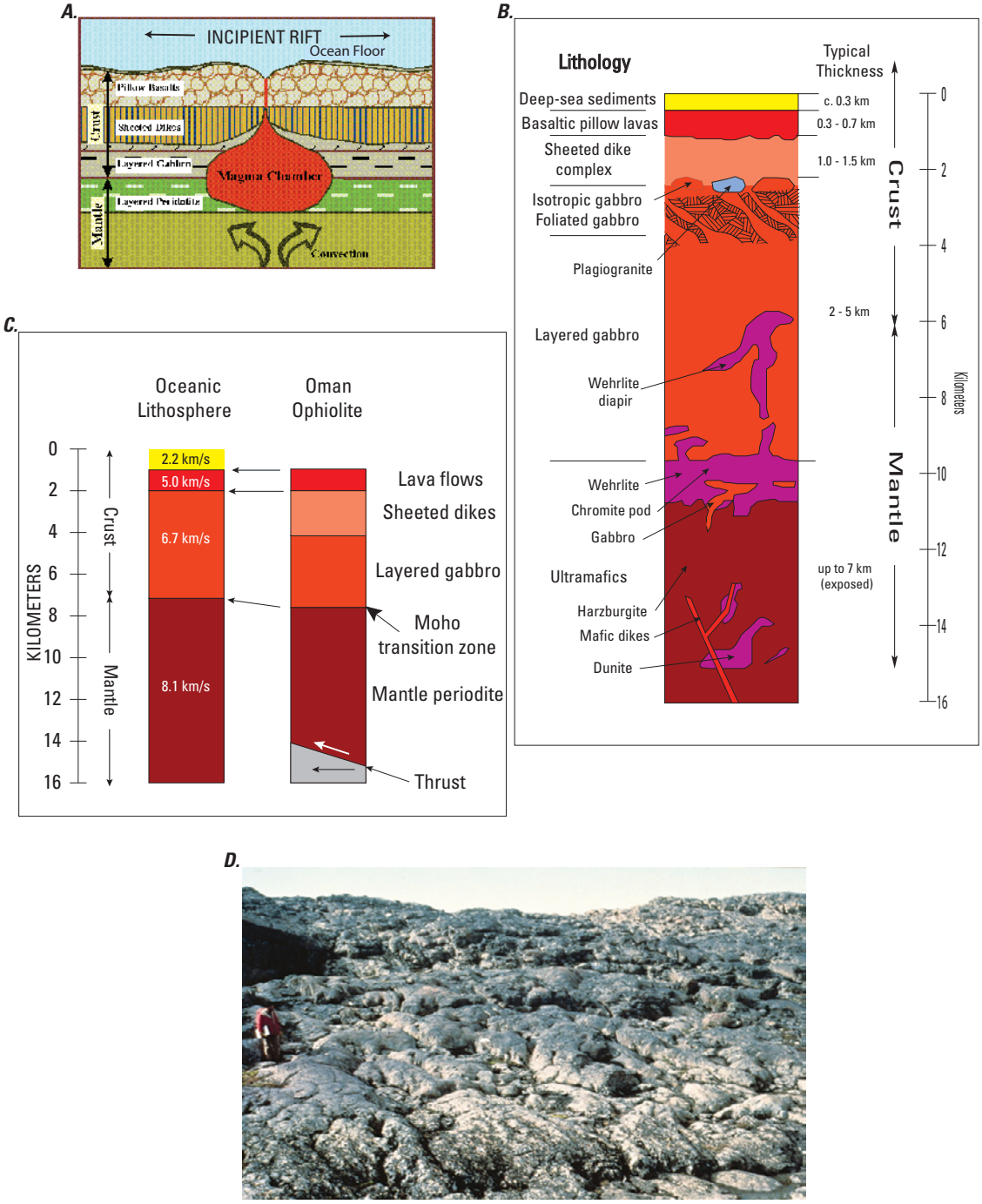

Figure 5–5. Tectonic setting and stratigraphy of mafic-ultramafic volcanogenic massive sulfide deposits. *A.* Generalized diagram showing the tectonic setting for mafic-ultramafic lithofacies (modified from Galley and Koski, 1999). The sheeted dikes and upper pillow basalt flows represent magma in transit to or on the surface whereas the layered gabbro and peridotite represent different parts of the upper mantle magma chamber, namely the crystallized magma and the depleted upper mantle under the magma chamber, respectively. *B.* Generalized stratigraphic column with associated typical thicknesses of an ophiolite sequence showing the main stratigraphic components http://www.geol.lsu.edu/henry/Geology3041/lectures/13MOR/MOR.htm); *C.* Comparison of the oceanic lithosphere with the Oman Ophiolite, the largest ophiolite sequence in the world (modified from http://geogroup.seg.org/oman_ophiolite.htm); *D.* Photograph of a 2-Ga ophiolite in Quebec, Canada showing basaltic pillow lava surface (from http://www.earth.northwestern.edu/people/seth/107/Ridges/ophiolite.htm). (Harper, G.D., 1984).

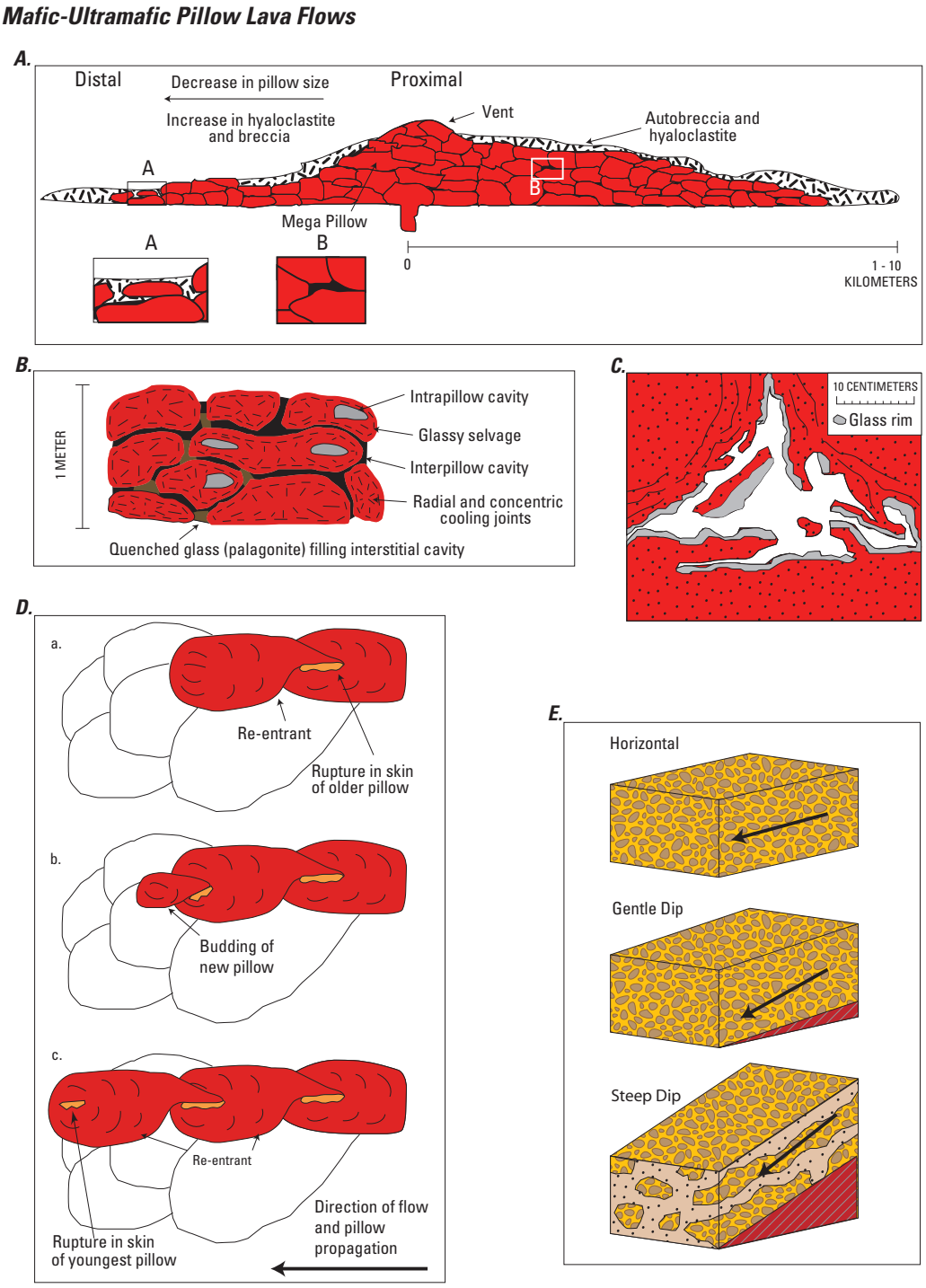

Figure 5–6. Series of figures highlighting features of mafic-ultra mafic pillow lava flows. *A*, Idealized cross section through a pillow (tube-fed) basalt-andesite flow showing flow morphology and structures typical of proximal and distal facies. Inset A illustrates autobrecciation of pillows; inset B illustrates densely packed pillows surrounding a mega-pillow or lava tube. Vertical exaggeration is approx. 3x. From Gibson and others (1999). *B*, Detail of pillows. In cross section, pillows can vary from 10 cm spheres to large forms several meters across; they are usually several tens of centimeters in diameter. From Cas and Wright (1988); modified from Hargreaves and Ayres (1979). *C*, Close-up sketch of pillow lavas showing glassy rims or selvages spalling off, creating fine-grained material. From Walker (1992). *D*, Cross section illustrating development of re-entrant selvages by budding of a new pillow. After Hargreaves and Ayres (1979). *E*, Schematic block diagrams illustrating the morphological changes of pillow flows with change in slope. Modified from Walker (1992).

pillow form (Walker, 1992). The exterior skin on each pillow is quenched, preventing coalescence into a massive form (fig. 5–6*B*). Slope angle also exerts control on the size and aspect ratio of pillows (see Ross and Zierenberg, 1994) (fig. 5–6*E*).

Pillow flows of basaltic composition are relatively small in size, are typically smooth surfaced, and are inferred to have inflated mainly by stretching of their skin (Walker, 1992). Gibson and others (1999) subdivided pillow lavas into two units: a pillow lava unit and a less abundant pillow breccia unit. A cross section of a pillow lava sequence shows densely packed "pillows" separated by thin glassy selvages and hyaloclastite breccia (fig. 5–4*B,* fig. 5–6*B*). The lava flow advances as a prograding pillow delta fed by bifurcating and meandering tubes that feed a variable supply of magma to the flow front; this is reflected in the variable dimensions of individual pillows. Proximity to source vent and sequence in eruption interval also contribute to the physical form of the flow. Monolithic breccias at the top and terminus of a pillow lava and occurring between pillows are interpreted as autobreccias and represent in situ fragmentation of pillows, pillow budding, spalling of lobes, gravitational collapse on steep slopes, and later granulation of sideromelane pillow crusts.

Komatiites are magnesium-rich volcanic rocks that are found as lava flows, tuffs, hyaloclastites, and autobreccias (Gibson and others, 1999). Ultramafic (>18 percent MgO) komatiitic flows are interpreted as lavas erupted at high temperatures (1,400–1,700 °C) and very low viscosities (Huppert and Sparks, 1985), the latter factor contributing to the extensive aerial extent and sheet-like form of komatiitic flows. The high temperatures permit the flows to melt and thermally erode their bases and deepen their flow channels. Huppert and Sparks (1985) showed that komatiitic melts have Reynolds numbers in excess of the critical value of 2,000 and are emplaced by turbulent flow, which would also enhance thermal erosion and contribute to heat loss and high cooling rates. While association of VMS deposition in komatiitic flows is uncommon, komatiitic flows are exposed at the base of the volcanic succession at the Kidd Creek district in Ontario, Canada. Whether they somehow contributed to the giant VMS complex at Kidd Creek is unknown, as the komatiites are separated from the VMS deposits by about 350 m of overlying strata containing rhyolitic domes, cryptodomes, and volcaniclastic rocks (Prior, 1996; Barrie and Hannington, 1999). Small VMS deposits are associated with tholeiitic and komatiitic basalts in the Kidd-Munro assemblage.

As shown in figure 5–1*A*, VMS bodies may be completely enclosed by mafic pillow flows above sheeted dikes. Thick (approx. 0.4 km average) sections (figs. 5–5*A*-*C*) of sheeted dikes are present below the typical pillow lava flow-dominated sequence in ophiolites. Sheeted dikes represent the conduits transporting magma to the surface to pillow flows. Typical mineralization in the dikes is limited and most of the massive sulfide mineralization is localized in the pillowed lavas.

Bimodal-Mafic Volcanic Suite (Incipient-Rifted Intraoceanic Arcs)

Intraoceanic rifted bimodal arcs make up approximately 17,000 linear km (40 percent) of the global volcanic arc system. Volcanism mostly occurs on the seafloor; however, occasionally the upper part of the volcanic edifice becomes emergent and forms islands (Leat and Larter, 2003). In contrast to subduction systems at continental margins, the intraoceanic subduction systems generally have a shorter history of subduction and are distinct in that magmas are not contaminated by ancient sialic crust and have little or no continental component. Intraoceanic arcs form on oceanic crust produced either at mid-ocean ridges or in back-arc spreading centers and erupt a predominantly basalt bimodal volcanic suite that can contain up to 25 percent felsic lava flows and domes. Intraoceanic arc volcanism is truly bimodal. Basaltic and basalt andesitic mafic lavas are dominant; subordinate units include silicic lavas. Intermediate composition volcanic rocks (such as andesite) are essentially absent from these terranes.

Volcanic products are lava flow dominated and include basaltic pillow and massive lava flows, felsic lavas flows, and felsic domes (figs. 5–1*B*, 5–7). Summit calderas, typically 3–7 km in diameter, are common in bimodal-mafic volcanic systems (Leat and Larter, 2003). Ancient and modern subaqueous calderas have been identified in shallow and deep marine environments and are primary hosts of VMS deposits (for example, Gibson and Watkinson, 1990; Syme and Bailes, 1993). Calderas are volcano-tectonic collapse structures that form because of the evacuation of voluminous amounts of high-level magma (Mueller and others, 2009). Volcanism associated with caldera formation can be dominated by either effusive eruptions (producing lobe-hyaloclastite flows, domes, blocky lavas, or shallow intrusions) or explosive activity (producing pyroclastic flow, surge, and fall deposits).

Effusive Dominated Subaqueous Calderas in the Bimodal-Mafic Associations

In bimodal mafic systems, subaqueous calderas form at the summit of long-lived fissure-fed shield volcanoes, have a variety of shapes and aspect ratios, and vary in their level of complexity (Franklin and others, 2005). These collapse structures can cover up to tens of square kilometers. The stratigraphic sequences from these systems contain compositionally and texturally diverse lavas and volcaniclastic rocks, reflecting a broad spectrum of eruption styles and emplacement processes (McPhie and Allen, 1992).

The subaqueous Hunter Mine caldera in the Archean Abitibi greenstone belt is a 5–7-kilometer-wide felsic-filled caldera that developed over a 6 m.y. time span (Mueller and others, 2009) and is presented as one example of an effusive-dominated caldera forming system. Caldera formation was followed by renewed rifting and the emplacement of massive and pillowed komatiitic lavas. Silicified mudstone, banded

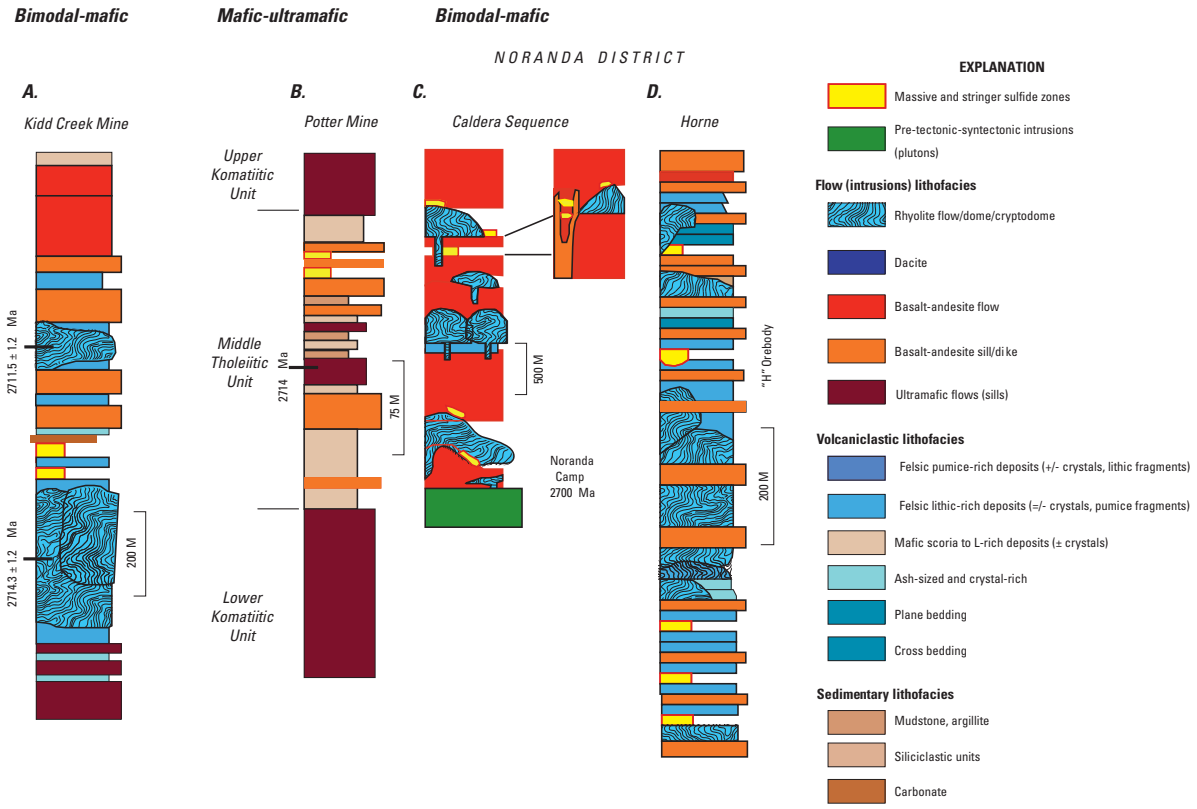

Figure 5–7. Composite stratigraphic sections for various areas hosting volcanogenic massive sulfide mineralization in the bimodal mafic suite. *A–B*, Kidd Creek Mine and Potter Mine contain both flow and volcaniclastic lithofacies assemblages. At Potter Mine, rhyolitic flows and volcaniclastic units are absent; abundant basaltic pyroclastic strata are present. From Gibson and Gamble (2000); geochronology from Bleeker and Parrish (1996). *C–D*, Schematic stratigraphic sections from the Noranda District through intracaldera flow-dominated lithofacies (*C*) and the rhyolitic volcaniclastic-dominated lithofacies succession that hosts the Horne deposit (*D*) is located along the southern structural margin of the Noranda caldera (modified after Gibson, 2005). From Franklin and others (2005). The Noranda District is considered to be bimodal maffic. (Ma, mega-annum)

iron formation, bedded felsic hyaloclastite, and abundant Bouma sequences on depositional contacts above komatiitic flows testify to submarine volcanism occurring at >500 m water depth (Mueller and others, 2009). Caldera formation in the Hunter Mine caldera was complex, involving at least two caldera-forming events separated in time by the intrusion of a gabbroic sill. The 5–7-km-wide caldera contains numerous synvolcanic faults and fractures; vertical offsets can be as much as 20 m (Mueller and others, 2009). The initial caldera formational stage included emplacement of three distinct lithofacies: (1) felsic lavas, domes, and autoclastic breccias (about 70 percent); (2) subaqueous pyroclastic deposits and reworked equivalents (Mueller and others, 2009); and (3) a 5–to 7–km-wide section of north-trending rhyolitic dikes that can be traced for several kilometers, representing the final lithofacies. A shallow, intracaldera, 1–km-thick gabbroic sill was subsequently emplaced during a period of tectonic extension, possibly associated with caldera resurgence (Wharton and others, 1994). The formation of a second caldera was marked by a trend toward more mafic-dominated magmatism. Three distinct lithofacies also are associated with the second caldera-forming stage: (1) felsic and mafic lava flows and domes, (2) volcaniclastic rocks and banded iron-formations, and (3) mafic dikes and sills.

Further evidence for long-lived multiphase caldera formation has been documented at the Normetal caldera, Quebec, where Mueller and others (2009) identified 5 stages of caldera formation and infill (fig. 5–8). Here, the volcanic sequence began with emplacement of primarily basaltic and basalt andesitic massive and pillow flows in water depths in excess of 500 m. Later dacite lavas were emplaced near the summit of the shield volcano. In stage 2, caldera formation followed with emplacement of rhyolitic lavas and volcaniclastic material. Later in stage 3, andesite-dacite flows and breccias and thick rhyolite flows were emplaced as individual volcanic centers. The fourth stage was constructive with the emplacement of high-level rhyolite endogenous domes. Deposition of deep-water volcaniclastic turbidites and shale sedimentation followed and represents a period of deconstruction and partial collapse of the volcanic edifice. The final phase of volcanic activity included emplacement of mafic and felsic flows with tuff, lapilli tuff, and lapilli tuff breccia (Mueller and others, 2008, 2009).

Volcaniclastic units are subordinate in the bimodal-mafic environment, but both mafic and felsic volcaniclastic rocks with sedimentary rocks including immature wacke, sandstone, argillite, and debris flows occur locally (fig. 5–7) (Franklin and others, 2005). The effusive nature of the dominant lava flow lithofacies associations suggest eruptive sources such as single and composite shield-like volcanoes fed by subvolcanic dikes, sills, and cryptodomes.

Up to 25 percent of the lavas erupted in young, intraoceanic arcs are subaqueous felsic lobe-hyaloclastite flows, cryptodomes (shallow subvolcanic intrusions), and blocky lavas and domes; all are associated with VMS deposits in ancient associations (fig. 5–8) (Gibson and others, 1999; Gibson, 2005; Mueller and others, 2008, 2009). Occasionally, the lavas form broad shield forms with slopes up to 15°. Commonly, the felsic lavas are hundreds of meters thick, have flowed up to 10 km from source, and have steep flow fronts (up to 40°) (Cas, 1992). One such felsic lava in a mafic-bimodal suite has been mapped in an Archean volcanic complex at the Noranda district in northwestern Quebec. Here the cauldron or rift graben is underlain by a large multiphase subvolcanic intrusive complex. The complex is dominated by mafic flows into which discrete felsic dome complexes have been emplaced along synvolcanic fault systems. In the Noranda cauldron, these faults are defined by dike swarms associated with the underlying subvolcanic system (Gibson and Galley, 2007) which fed the eruptions. The felsic lobe-hyaloclastite flow best typifies felsic lavas found in mafic-bimodal complexes.

Felsic Lobe-Hyaloclastite Flows in Bimodal-Mafic Associations

Felsic lobe-hyaloclastite flows in the Noranda complex are interpreted as fissure-fed systems that formed gentle sloped (10–20°) shield volcanoes or plateaus as much as 500 m high with individual lava flows restricted to <5 km from their vents (Gibson and Watkinson, 1990). The flows formed domes or "lobes" that vented from their summits above the sediment-water interface and above their feeding fissures, which preferentially follow synvolcanic faults (fig. 5–9). The lobes are irregular or podiform in shape, may be up to tens of meters in diameter, and may show a distinct lithologic zonation described by Cas (1992).

Three primary facies (massive, lobe-hyaloclastite, and breccia) are associated with felsic lobe-hyaloclastite flows and relate to distance from the vent (fig. 5–9) (Gibson and others, 1999). Each facies represents a continuum in the evolution of textures and structures in response to cooling and quench fragmentation during the eruption of lava into water. Massive facies are proximal flows and are represented by lobes >100 m in length composed of massive, flow-banded, and brecciated lava. At or next to the vent, the massive facies are dome-like. The lobes in massive facies typically have columnar, jointed, and glassy interiors which grade outward into chilled, flow-banded, and amygdaloidal vitrophyric exteriors. The lobe-hyaloclastite facies consists of irregular lobes, 2 to 100 m in length, engulfed by hyaloclastite and brecciated flow-banded lava (fig. 5–9*A*). Hyaloclastite refers to the clastic aggregate that forms through non-explosive fragmentation and disintegration of quenched lavas and intrusions (Rittman, 1962; Yamagishi, 1987; McPhie and others, 1993). The breccia facies is distal and composed of a poorly sorted carapace breccia and a crudely layered to redeposited flank breccia (Gibson and others, 1999). At these distal exposures, lobes appear to physically range from in situ fractured clasts of "jigsaw-fit" obsidian to obsidian hyaloclastite breccias with rotated clasts (fig. 5–9*A*) (Cas, 1992). Each facies is interpreted as

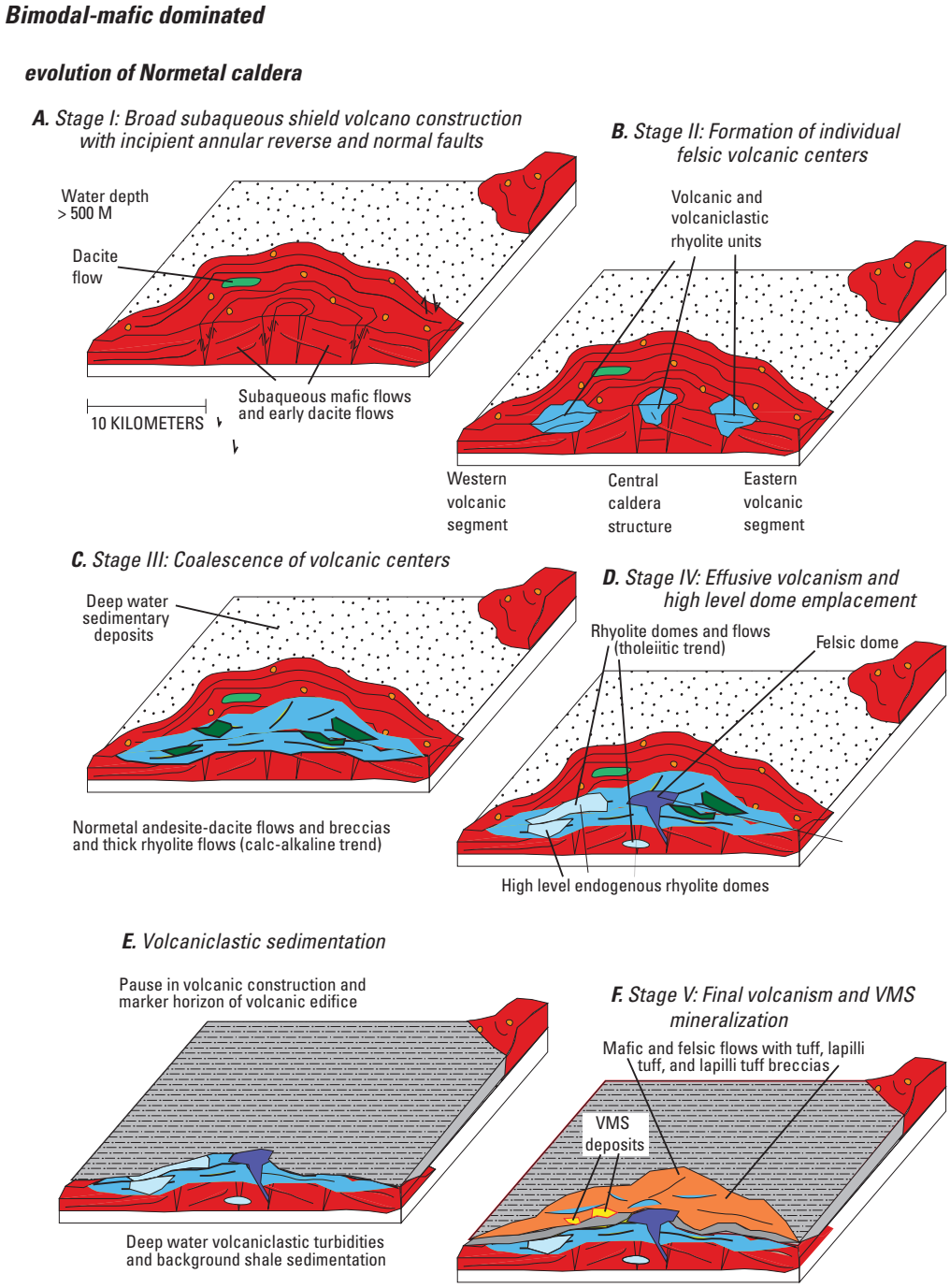

Figure 5–8. Paleogeographic reconstruction of the bimodal-mafic dominated evolution of the Normetal caldera from a subaqueous shield volcano to a piston-type caldera. *A*, Stage I. Broad subaqueous shield volcano construction with incipient annular reverse and normal faults. *B*, Stage II. Formation of individual felsic volcanic centers. *C*, Stage III. Coalescence of volcanic centers. *D*, Stage IV. Effusive volcanism and high level dome emplacement. *E*, Volcaniclastic sedimentation. *F*, Stage V. Mine sequence. From Mueller (2008).

Bimodal-mafic dominated
felsic lobe hyaloclastite facies

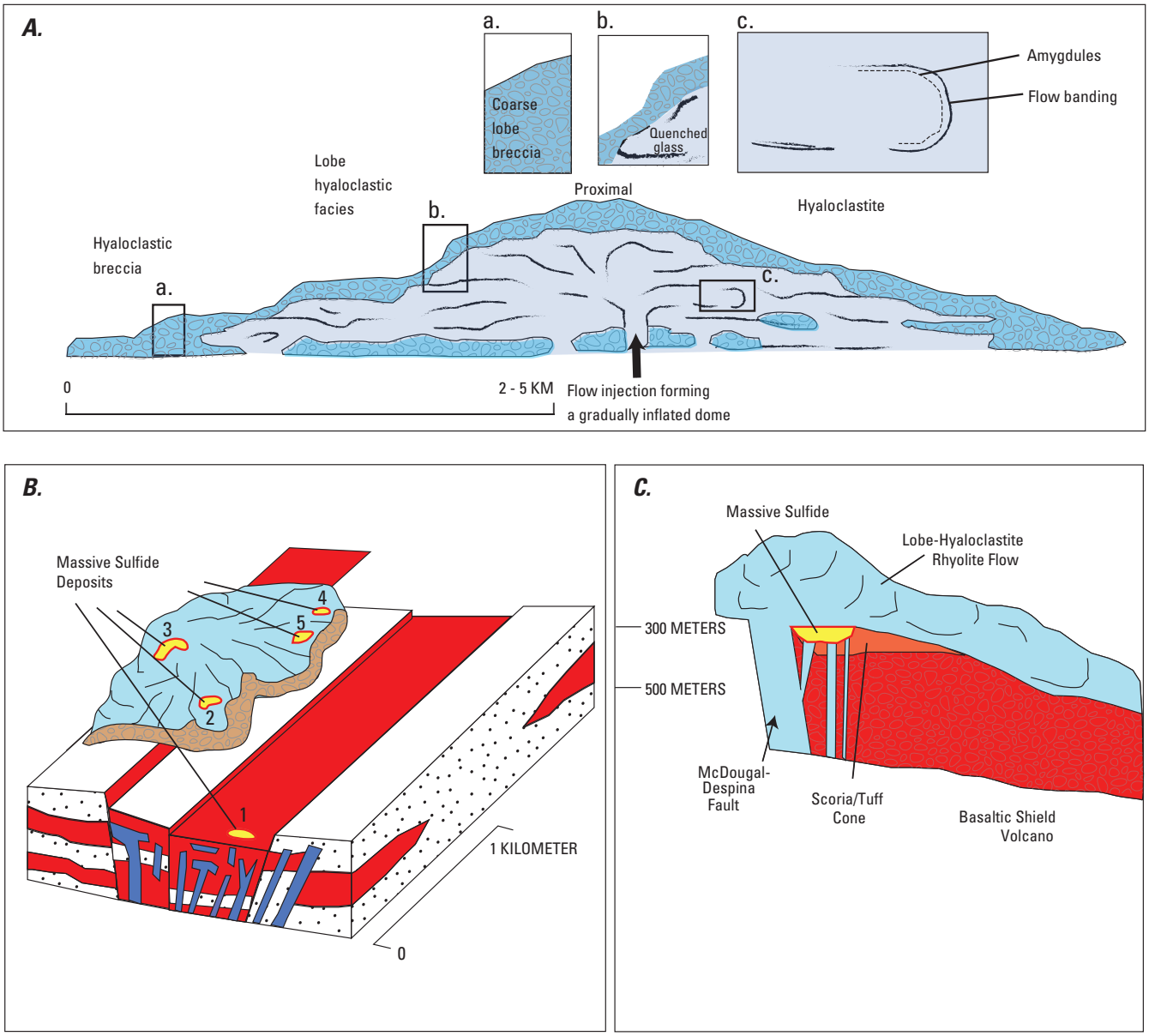

Figure 5–9. Features associated with bimodal-mafic association, specifically the felsic lobe hyaloclastite facies. *A*, Schematic cross section through a rhyolitic lobe-hyaloclastite flow showing flow morphology and structures typical of proximal and distal facies (modified after Gibson and Watkinson, 1990). *B*, Oblique perspective of the Noranda complex showing the volcanic reconstruction of contemporaneous rhyolitic and basaltic andesite flows of the Amulet Formation within a graben or fissure defined by massive flows and dikes of the Old Waite Paleofissure. The volcanogenic massive sulfide (VMS) deposits, marked by red-rimmed yellow blobs, are localized within and along the fissure and are associated with both the rhyolitic and andesitic basalt flows; numbers 1–5 correspond to VMS deposits (from Dimroth and others, 1985; Gibson and Watkinson, 1990). *C*, Cross section perspective through the McDougal-Despina fault, the feeder dike, and relationships between the lobe-hyaloclastite flow, the massive sulfide deposit, and the shield volcano and tuff cone.

representing a continuum in the evolution of textures and structures formed in response to cooling and quench fragmentation during the eruption of lava into water.

The massive facies lack hyaloclastite, which suggests a general lack of interaction with water. Rather, this facies most likely evolved by successive injections of magma lobes into a gradually inflating dome. Individual lobes are identified by stringers of amygdules and flow-banded margins (fig. 5–9*A*, inset c) (Gibson and others, 1999) and a lack of glassy selvages. In contrast, flowing lava in contact with water forms glass-like selvages on exterior lobes, which reflect rapid quenching (Gibson and others, 1999). These glass selvages are the source for the fine-grained clastic materials that form the hyaloclastite component of the lobe-hyaloclastite facies (Gibson and Galley, 2007).

The breccia subfacies is composed of matrix-supported hyaloclastite that has formed through quench fragmentation and contains clasts of flow-banded and massive felsic lava lobe fragments. Two subfacies of the breccia facies have been recognized: carapace breccia, which covers the flow, and hyaloclastite breccia, which forms at the distal edges and perimeter of the flow. The carapace breccia phase contains chaotically distributed clasts of flow-banded felsic flows. Here, the absence of bedding and grading and a lack of broken crystals indicate an origin derived through autobrecciation, which involves the non-explosive fragmentation of flowing lava (McPhie and others, 1993). The more distal breccia subfacies is the flank breccia (fig. 5–9*A*) and consists of clast-supported beds of coarse lobe fragments in a fine-grained hyaloclastite matrix (Gibson and others, 1999) interbedded with plane-bedded hyaloclastite deposits. The areal extent and volume of flank breccias are limited and represent the outer-most part of the lobe-hyaloclastite flow where slumping and later redeposition of autobreccia and hyaloclastite as subaqueous mass flow deposits are controlled by the low relief and gentle slope of the flows.

Quaternary, subglacial lobe-hyaloclastic flows of dacite and rhyolite composition in Iceland have similar characteristics as those found in the geologic record (Furnes and others, 1980). In the Iceland flows, however, some are associated with pumiceous hyaloclastite containing gray pumice and obsidian fragments that may have been emplaced as Surtseyian or Subplinian to Plinian eruptions (Furnes and others, 1980). Furnes and others (1980) interpret these flows as being emplaced in a shallow (<200 m) subglacial lake. The lack of pumiceous hyaloclastite in subaqueous lobe-hyaloclastite flows observed in the geologic record may be a function of their emplacement in deeper water (Gibson and others, 1999).

Lobe-hyaloclastite flows have many of the same physical characteristics as tube-fed pahoehoe or pillow lavas and are interpreted as being the silicic analogue for the better-known mafic process. Lobe-hyaloclastite flows advance in tube fed systems but because of higher viscosity and lower temperatures develop somewhat different morphologies. These lobes look very similar to basaltic pillow lavas but are developed on a much larger scale. In comparing the physical characteristics of the flow lobes in the massive facies with flow lobes contained in the breccia facies, both have very similar textures, structures, and amygdule content, suggesting that the hyaloclastitic matrix and glass selvages had excellent thermal insulating properties which protected and preserved these features (Gibson and Galley, 2007).

The felsic lobe-hyaloclastite flows represent the later and more evolved stages of submarine basaltic fissure vent systems, which form large shield volcanoes on the ocean floor. In ophiolite complexes, such as Oman and Semail, lobe-hyaloclastite flows are volumetrically small and occur in the upper mafic volcanic sequences of these complexes. Often, collapse calderas occur at the summit of large shield volcanoes and are filled by fissure-fed lobe-hyaloclastite flows emplaced as isolated domes; the lobe-hyaloclastite flow is the dominant lava flow morphology for felsic lavas in these subaqueous environments. In the upper sections of the Oman ophiolite complex, the fissures feeding the felsic lobe-hyaloclastite flows are oriented perpendicular to the inferred orientation of the spreading ridge (Gibson and others, 1999). It should be noted that VMS deposits in both intraoceanic arcs (where mafic-bimodal volcanic suites are the dominant lithofacies) and in continental arc and back-arc terranes (where felsic-bimodal volcanic suites dominate) form a variety of lithofacies within each individual complex.

Other Silicic Flows and Domes in Bimodal-Mafic Associations

Small-volume silicic lava flows and domes often are emplaced as endogenous domes immediately above feeding fissures and flow as viscous blocky lava flows <2 km from their vents. Like their subaerial equivalents, these flows have steep flow fronts (20–70°), a rugged form, and develop into a proximal and distal facies (Gibson and others, 1999) (fig. 5–10). In the submarine setting, three facies develop: a massive central facies, a carapace breccia facies, and a distal flank facies, similar in nature as described above for felsic lobe-hyaloclastite flows (Gibson and others, 1999). At the Millenbach-D68 lava dome in the Noranda cauldron complex, Quebec, Canada, 15 VMS deposits are associated with silicic flows immediately above their feeding vent fissures, which later acted as the conduits for ascending hydrothermal fluids. Figure 5–10 identifies these facies.

Another bimodal mafic VMS deposit, Bald Mountain (Maine, USA), formed in deep marine, rift-controlled basins or calderas (Busby and others, 2003). The 5-km-thick volcanic sequence was deposited in three major episodes (fig. 5–11). An early volcanic episode during rapid extension was dominated by a high rate of eruption of basaltic flows and development of breccia hyaloclastites. This episode was followed by an ignimbrite-producing, caldera-forming episode and development of VMS mineralization and a final episode that included eruption of rhyolitic lavas and emplacement of subvolcanic intrusions (Busby and others, 2003; Goodfellow and others, 2003).

Siliciclastic Felsic Domes

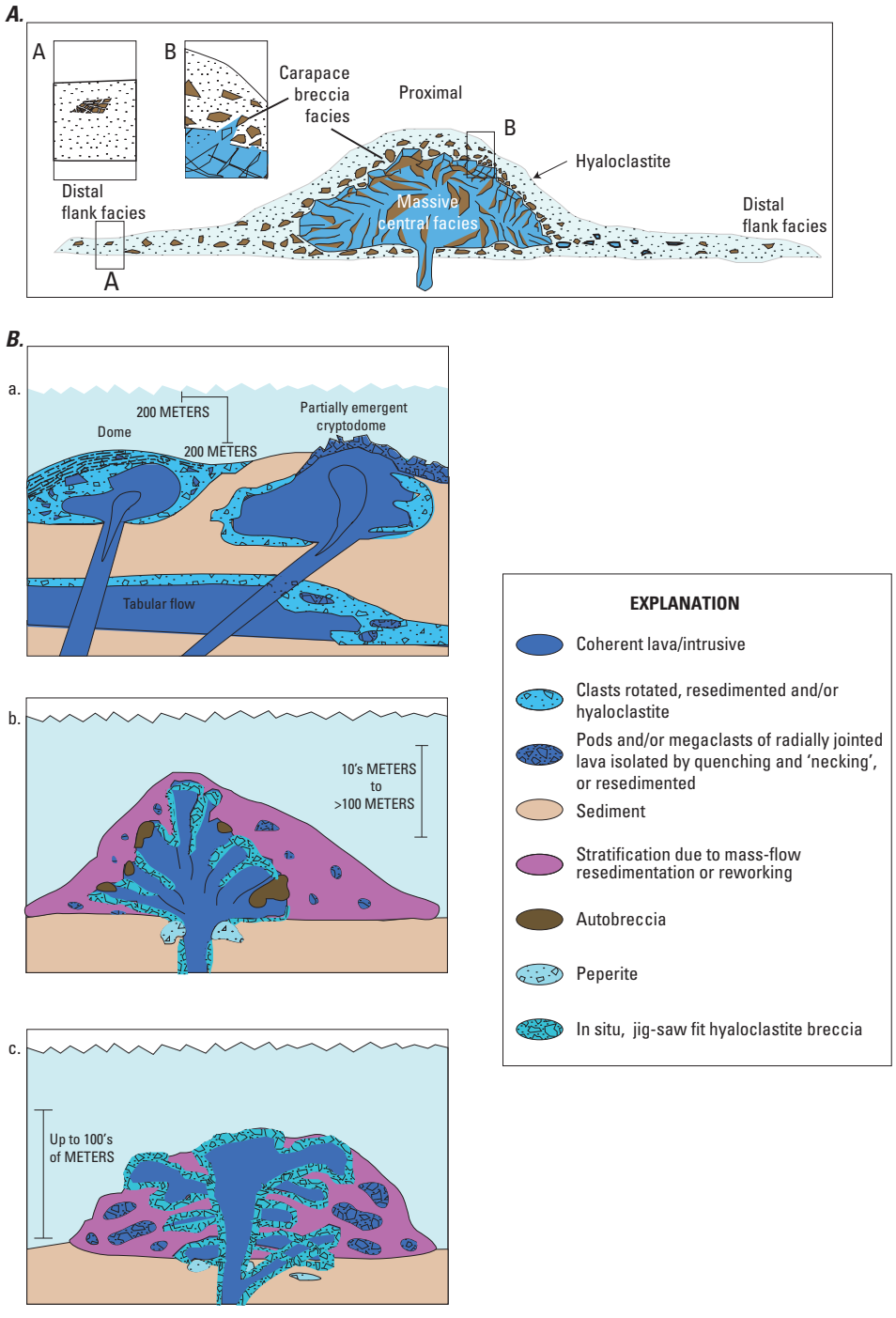

Figure 5–10. Volcanic domes common in a siliciclastic felsic suite. *A*, Schematic cross-section through a blocky rhyolitic flow depicting flow morphology and structures common for proximal and distal facies (after Gibson, 1990). *B*, Silicic lavas can be divided into three main types. (a) Various forms of silicic submarine lavas and intrusive domes (from Allen, 1988). (b) Schematic representation of the internal form and facies of a vent-top silicic submarine dome (after Pilchler, 1965; Yamagishi, 1987). (c) Schematic sketch of the internal form and facies of a subaqueous lava lobe-hyaloclastite complex (after de Rosen-Spense and others, 1980; Furnes and others, 1980; Yamagashi and Dimroth, 1985). From Cas (1992).

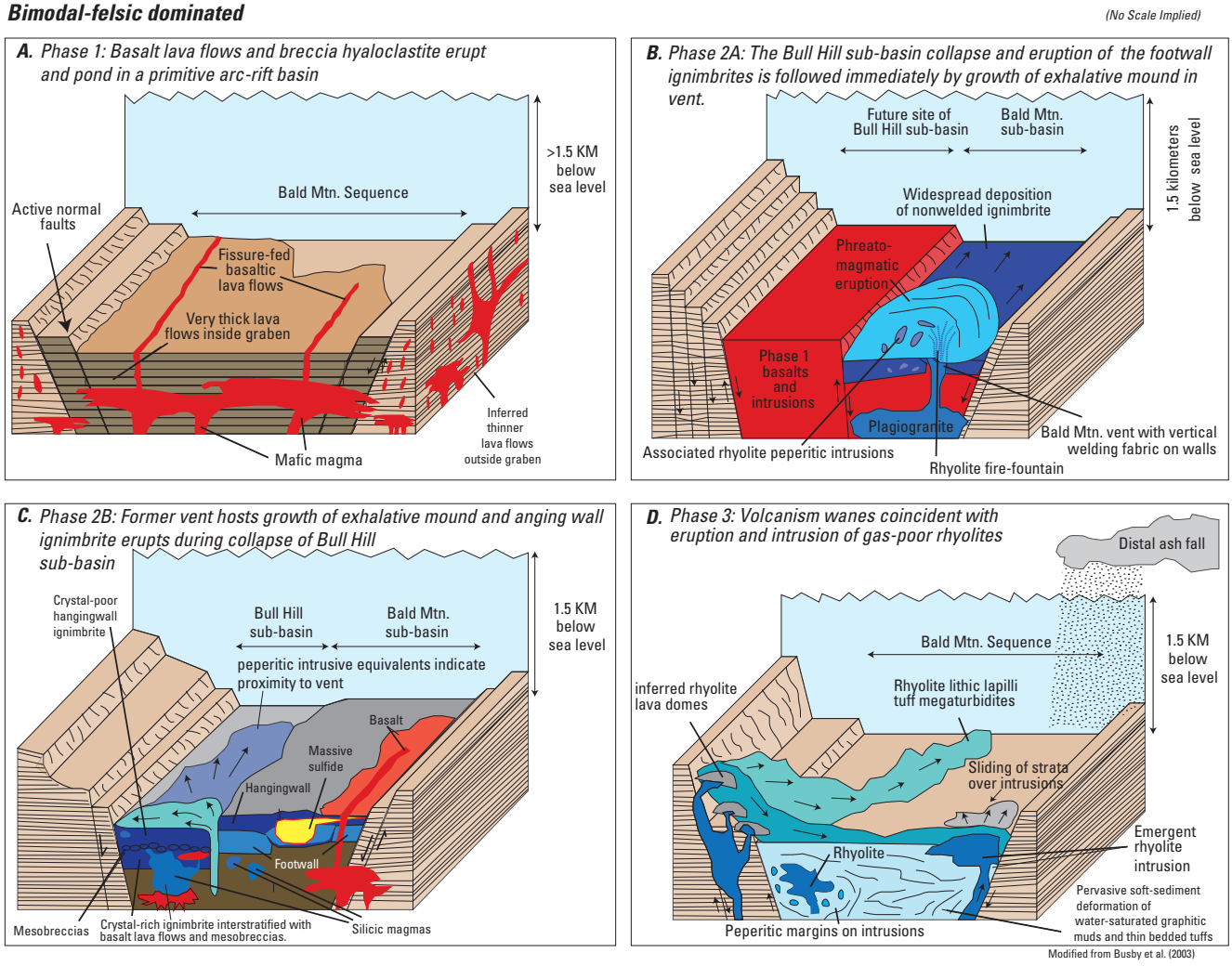

Figure 5–11. Schematic evolution of the bimodal-felsic dominated Bald Mountain sequence. (Cross sections are based on data presented in Busby and others, 2003.) *A*, Phase 1. Outpouring and ponding of basalt lava flows and breccia hyaloclastite in a primitive arc basin. *B*, Phase 2A. The collapse of Bald Mountain sub-basin and eruption of footwall ignimbrite was followed immediately by volcanogenic massive sulfide (VMS) mineralization of an exhalative mound within the vent structure. *C*, Phase 2B. As the Bull Hill sub-basin collapsed, the pyroclastic flow forming the hangingwall ignimbrite erupted. *D*, Phase 3. The waning stages of volcanism were represented by the eruption of gas-poor rhyolites emplaced as lobe-hyaloclastite flow capping VMS mineralization. Modified from Busby and others (2003).

Major breaks in volcanic activity allowed for the deposition of laminated carbonaceous interbedded mudstones. Based on fluid inclusion data from the VMS deposit (Foley, 2003) and sedimentologic features in the deposits at Bald Mountain, Busby and others (2003) suggest that the entire 5–km-thick section of the Bald Mountain sequence was emplaced in very deep water at submarine depths in excess of 1,450 m.

Bimodal-Felsic Type (Incipient-Rifted Continental Margin Arcs and Back Arcs)

Modern continental margin arcs and related back arcs have a global length of approximately 25,600 km (Von Huene and Scholl, 1991) and are hosts to felsic volcanic rocks (35–70 percent total volume of volcanic strata), mafic volcanic rocks (20–50 percent total volume of the volcanic strata), and about 10 percent terrigenous sediment (Franklin and others, 2005). Modern examples include the Okinawa Trough, the Woodlark Basin, and the Manus Basin (table 2–1). In these environments, submarine felsic volcaniclastics and lavas dominate with subordinate volumes of basaltic and (or) basalt andesitic flows, dikes, and sills (Franklin and others, 2005). This association hosts some of the most economically significant VMS deposits (Galley and others, 2007) that have developed in a variety of lithofacies (Franklin and others, 2005). Magmas in these environments are strongly influenced, both physically and chemically, by continental crust and include a broad spectrum of compositions including basalts, basaltic andesites, andesites, dacites, and rhyolites. Volcanism in the early stages of development of a continental arc may begin in a subaqueous environment (such as at Manus and Woodlark Basins). The volcanic systems and the subduction process here often have a prolonged history and continue to develop into large, massive subaerial volcanoes. The subaerial felsic-bimodal volcanic suite contributes clastic volcanic material that has been fragmented and dispersed by any transporting agent, deposited in any environment. This clastic material may be mixed in any significant portion with non-volcanic fragments into the subaqueous environment and redeposited as volcaniclastic material (Fisher and Schmincke, 1984).

Volcanism in incipient-rifted continental margin arcs and back arcs is focused at newly formed rifts. Volcanism begins with emplacement of basaltic massive and pillow lavas, forming large submarine shield volcanoes. As the magmatic system evolves, volcanism becomes more silicic, gas-rich, and explosive and the resulting subaqueous eruptions have abundant pyroclastic material. The explosive activity is interspersed with effusion of lava flows and domes and intrusions of dikes and sills feeding individual eruptions. Interspersed with constructional volcanic processes are those processes associated with structural or magmatic collapse of the volcanic edifices, including debris flows, pyroclastic fall and flow deposits, mud flows, and lava domes, some of which are subaerial and eventually contribute to the subaqueous bimodal-felsic stratigraphic sequences.

Submarine calderas form in either shallow or deep marine environments and develop on both stratovolcanoes and composite volcanoes through large-scale pyroclastic eruptions. Consequently, pyroclastic lithofacies are an important component of the bimodal felsic suite. Pyroclastic lithologies are composed of magmatic ash and pumice, crystal fragments, and lithic clasts derived from the vent wall or incorporated from the underlying terrain during flow.

In the submarine environment, most volcaniclastic material is pyroclastic; however, fragmental material is also derived from autobrecciation, quench fragmentation, pyroclast fragmentation, and resedimentation (Cas, 1992). Physical characteristics of pyroclastic deposits vary between subaerial and submarine settings. In the subaerial environment, Plinian eruption columns are responsible for large pyroclastic-fall deposits and typically are accompanied by pyroclastic flows. Clast size in subaerial pyroclastic fall deposits vary systematically with distance from eruptive source and are a function of eruption column conditions, grain size, density of the various sized clasts, and prevailing wind direction (Walker, 1971; Sparks and others, 1973; Gibson, 2005). In contrast, the eruptive columns of explosive submarine eruptions can be completely subaqueous or become subaerial as a function of eruption intensity and water depth. Consequently, size sorting may involve both water and air. In comparison to subaerial deposits, subaqueous pyroclastic deposits are generally better sorted, are more limited in their aerial distribution, and are typically enriched in crystals and fragments at their base, with finer and ash-rich deposits at their tops. Like their subaerial equivalents, clast size and thickness of deposit varies systematically with distance from eruptive source. The subaerial component of the submarine eruption can produce large volumes of fine ash and cold pumice that are removed by flotation so that the resultant submarine deposits near the edifice may be pumice-depleted. (Gibson, 2005).

Explosive Dominated Submarine Calderas in Bimodal-Felsic Associations

The history of a well-studied and well-exposed Archean caldera is preserved in a 2- to 4-km-thick intracaldera volcanic sequence from the Sturgeon Lake caldera, Canada. The 30-km-wide Sturgeon Lake caldera has a 1– to 2–km-thick sequence of volcaniclastic debris and subaqueaous pyroclastic density flow deposits (Mueller and others, 2008) that overlie a thick (approx. 2 km) tonalite-diorite sill-like body. Caldera development advanced in four stages. Stage 1 was a shield-building phase that involved primarily mafic lavas with subordinate felsic breccia and volcaniclastite. Stage 2 was characterized by further caldera collapse associated with the emplacement of 650–1,300-m thick of pyroclastic deposits. This stage contains caldera wall collapse breccias, ignimbrites, bedded tuffs, and lapilli tuffs. Further caldera collapse is recognized in Stage 3 and is associated with the eruption of andesitic and dacitic flows, emplacement of endogenous

domes, and deposition of banded iron formation and volcaniclastic debris. Intra-caldera deposits were dominated by thick, pillowed andesitic flows and felsic lava domes. The final phase of caldera formation (Stage 4) was marked by the emplacement of basaltic andesite flows and volcaniclastic rocks filling the last remnants of the caldera (Mueller and others, 2008).

Estimates of water depths in which subaqueous explosive eruptions can occur are controversial (McBirney, 1963; Pecover and others, 1973; Sparks and Huang, 1980; Burnham, 1983; Kokelaar, 1986; Wohletz, 1986; Cas and Wright; 1987; Cas, 1992). McBirney (1963) noted that the critical point and specific volume changes of pure water control the depth at which submarine explosive eruptions can occur (fig. 5–3*A*). The critical point of water is defined as the pressure at which water is incompressible and the properties of vapor and liquid are indistinguishable (Cas, 1992). For pure water, the critical point is 216 bars (2.16×10^7 pascals [Pa]); for sea water with 3.5 percent NaCl, the critical point is 315 bars (3.15×10^7 Pa) (Sourirajan and Kennedy, 1962; Cas and Wright, 1988; Cas, 1992); thus, given the pressure gradient of water of approximately 1 bar (10^5 Pa) per 10 m water depth, the depth of the critical point in pure water is about 2,160 m and in seawater is about 3,150 m. These critical point depths represent maxima for subaqueous explosive activity because at greater depths magmatic water and heated seawater would be incapable of expansion (Cas, 1992). For most magmas, the practical maximum depths of explosive eruptions range between 500 and 1,000 m, and generally less than that because these are the depths at which a range of silicate melts become vapor-saturated (McBirney, 1963). Pecover and others (1973) estimated the maximum depth for hydrovolcanic eruptions is less than 700 m.

Recently, several pumice beds in the Izu-Bonin arc (Japan) and the Lau Basin near Tonga have been discovered at depths greater than 1,500 m (Cashman and Fiske, 1991; Fiske and others, 2001), which suggests that pumice erupted from relatively shallow submarine continental-arc and back-arc volcanoes can be redistributed into deeper water. The bulk density of dry, cold pumice is about 0.6 grams per cubic centimeter (g/cm^3), so subaerial pumice will float. However, hot (>700 °C) pumice erupted subaqueously will become saturated in the underwater eruptive column and sink to the seafloor (Whitham and Sparks, 1986). Pumice produced during submarine pyroclastic eruptions has a bulk density between 1.1 and 1.4 g/cm^3 (Kato, 1987) because air in vesicles is displaced by steam, which condenses on cooling and forms a partial vacuum or negative pressure that draws in the surrounding water and saturates the pumice fragments. Interconnected vesicles further enhance water saturation (Cashman and Fiske, 1991). In submarine explosive eruptions, vesicles are formed by exsolving magmatic gases (H_2O, H_2S, CO_2, CO, and H) and have no component of air. If the pumice cools quickly, it will be saturated before reaching the surface of the sea and will sink and be deposited on the seafloor.

Few submarine explosive eruptions have been witnessed. Four submarine volcanic eruptions from >100 m depths have been documented as later evolving into subaerial eruptions (Mastin and Witter, 2000). The plume of ejecta from the recently witnessed submarine explosive eruption of NW Rota-1 (517 m below the surface) in April 2006 ascended less than 100 m above the vent and did not breach the ocean surface. The maximum depth from which submarine pyroclastic material can reach the ocean surface remains unknown (Chadwick and others, 2008). The top of the eruption column of many deep marine eruptions is severely influenced by the drag on the particles imposed by seawater; thus, the vertical momentum will rapidly decrease with height above the vent. The containment of erupted pyroclastic material results in a large volume of pyroclastic transport downslope and deposition on the lower slopes of the volcanic edifice, as observed at NW Rota-1 (Chadwick and others, 2008).

Recent (April 2006 and April 2009) explosive submarine eruptions at a depth of 550–560 m on NW Rota-1 volcano in the Marianas Arc were witnessed and recorded using a submersible remotely operated vehicle (Chadwick and others, 2008, 2009). The NW Rota-1 volcano, one of many volcanoes located in this intraoceanic subduction zone where underwater volcanoes outnumber their subaerial counterparts 5:1 (Bloomer and others, 1989; Stern and others, 2003; Embley and others, 2004; Chadwick and others, 2008), is a basalt to basaltic andesite steep-sided cone. Its summit depth is at 517 m below sea level (bsl) and its base is at 2,800 m bsl; it has a diameter of 16 km (Chadwick and others, 2008). Previous eruptions at NW Rota-1 volcano were briefly witnessed in 2004 and 2005 but in April 2006 observations made over a week-long period showed that the eruption evolved from an effusive phase that culminated in explosive bursts of glowing red lavas ejected by rapidly expanding gases (Chadwick and others, 2008). Video footage and hydrophones allowed for correlation between observations and digital acoustic data. The eruptive style is akin to subaerial Strombolian activity driven by ascending pockets of magmatic gases that result in periodic phases of explosive activity. In the case of NW Rota-1, the primary magmatic gas that causes explosive activity is interpreted as H_2O, which has the highest potential for rapid thermal expansion at magmatic temperatures (Chadwick and others, 2008). In contrast, CO_2 is assumed to be relatively passive and rises as clear bubbles from explosive bursts (Chadwick and others, 2008). Syneruptive sulfur gases, mainly SO_2, were also released as clouds of molten sulfur that dropped as beads to the ocean floor. As noted, water is the dominant gas at NW Rota-1 and is driving the explosive nature of this eruption. This type of volcanism is surmised to be common for intraoceanic arcs.

Exposures of submarine pyroclastic deposits in the Mio-Pliocene Shirahama Group, Izu Penisula, Japan, a submerged continental arc, give insight into submarine volcanism at 3–6 Ma (Cashman and Fiske, 1991). The volcanic sequence is represented by a basal pyroclastic debris flow, a transition

zone, and a capping fall-deposit zone. The lower pyroclastic debris flow contains clasts of andesite with chilled margins; analyses of their thermal remanent magnetism indicates that they were hot (approximately 450 °C) when emplaced. Grain-size decreases systematically upward from the pyroclastic debris flow to the capping fall deposit. All units are extremely depleted in material with grain sizes less than 1 mm (figs. 5–12*A, B*) and are interpreted as being from the same eruption (Cashman and Fiske, 1991). The fall deposit contains lithic fragments, pumice fragments, and broken crystals and has a striking size bimodality; the pumice fragments are five to ten times larger than the lithic fragments. In a subaerial setting, the density difference between dry pumice (0.6 g/cm^3) and lithic fragments (2.4 g/cm^3) produces a 2:1 to 3:1 pumice diameter to lithic diameter ratio. In contrast, saturated pumice in a submarine eruption has a higher bulk density (1.1–1.3 g/cm^3). The small density difference between saturated pumice and seawater results in reduced terminal velocities and produces hydraulically equivalent pumice and lithic fragments that have diameter ratios of 5:1 to 10:1 (Cashman and Fiske, 1991). Cashman and Fiske (1991) plotted terminal velocity values versus spherical diameter and showed that, theoretically, submarine fall deposits can be distinguished from subaerial fall deposits by the diameter ratios between pumice and lithic fragments.

Insight into the evolution of a submarine siliceous caldera and its associated deep-water pyroclastic deposits is provided by the young (several thousand years) Myojin Knoll caldera located along the Izu-Bonin arc. The caldera has a flat floor 1,400 m below sea level with walls that are 500–900 m high (Fiske and others, 2001). An actively developing Kuroko-type VMS deposit, rich in Au and Ag, is located in the caldera wall. As depicted in figure 5–12*C*, five stages of volcanic evolution have been recognized. During the first stage a broad volcanic edifice was built, composed of individual rhyolite domes, lavas, and associated volcaniclastic material emplaced in a rift setting. The second stage was marked by the eruption of pumice from a central vent at about 600 m below sea level. The initial pumice eruption column rose nearly to sea level and subsequently sank, forming a broad apron of thick fallout debris. At the climax of the eruption, but prior to caldera formation, the eruptive column breached the ocean surface, producing large rafts of floating pumice which may have been accompanied by hot pyroclastic flows. During stage three, large volumes of pumice flowed downslope as pyroclastic gravity flows as the slopes of the edifice steepened. Stage four was represented by caldera collapse due to large scale evacuation of magma and the generation of large volumes of hot, ash-laden water. The final stage was marked by the emplacement of silicic dome complexes within the floor of the caldera (Fiske and others, 2001). This evolutionary sequence provides important insights into interpreting the volcanic lithofacies observed in ancient VMS bimodal felsic associations.

Volcaniclastic-Lithofacies Associations

The volcaniclastic lithofacies are dominated by felsic volcaniclastic material with subordinate mafic and felsic domes and their associated autobreccia, hyaloclastite, and redeposited equivalents, cryptodomes, and minor synvolcanic intrusions such as sills, dikes, and minor clastic sedimentary rocks (Franklin and others, 2005). Sedimentary rocks such as carbonaceous argillite, immature epiclastic volcanic wacke, and carbonate (Franklin and others, 2005) are related to this lithofacies. The volcaniclastic lithofacies associations, the bulk of which is volcaniclastic material interspersed with lava flows, domes, and synvolcanic intrusions, have an origin controlled by explosive eruptive processes. Sources for volcaniclastic materials can be explosive, producing pyroclastic fall and flow deposits, syneruptive and redeposited (often interbedded with terrigenous materials), or post-eruptive. The overwhelming volcaniclastic component present in the volcaniclastic lithofacies is evidence of a volcanic architecture created by development of a central volcanic complex composed of single or composite submarine volcanoes (Franklin and others, 2005). The upper lithologies in this suite contain a very thick sequence of primary pyroclastic units that fill large collapse calderas. These lithologies are exposed in both the bimodal-mafic volcanic suite at the Sturgeon Lake caldera and the Hunter caldera, and the bimodal-felsic suite at the Roseberry and Hercules, Bald Mountain, and Bergslagen deposits. Some of these pyroclastic units are greater than 1 km in thickness, are areally extensive, and have volumes of as much as 50 km^3.

Sedimentary-Lithofacies Associations

Terrigenous clastic sedimentary rocks, such as wacke, sandstone, siltstone, mudstone, and carbonaceous mudstone dominate the sedimentary lithofacies association. Subordinate rocks include chert, carbonate, marl, and iron formation (Franklin and others, 2005). Volcanogenic massive sulfide deposits are spatially associated with volcanic rocks, including mafic and felsic lava flows, domes, cryptodomes and associated autobreccia, hyaloclastite, and peperite. Volcanism may occur as synvolcanic intrusions where dikes, sills, and cryptodomes are emplaced into epiclastic sediments. A common theme in sediment-dominated successions is that the VMS deposits occur within small volcanic centers that occupy small subsidence structures; these, in turn, are located in a larger sediment-filled extensional basin (Franklin and others, 2005).

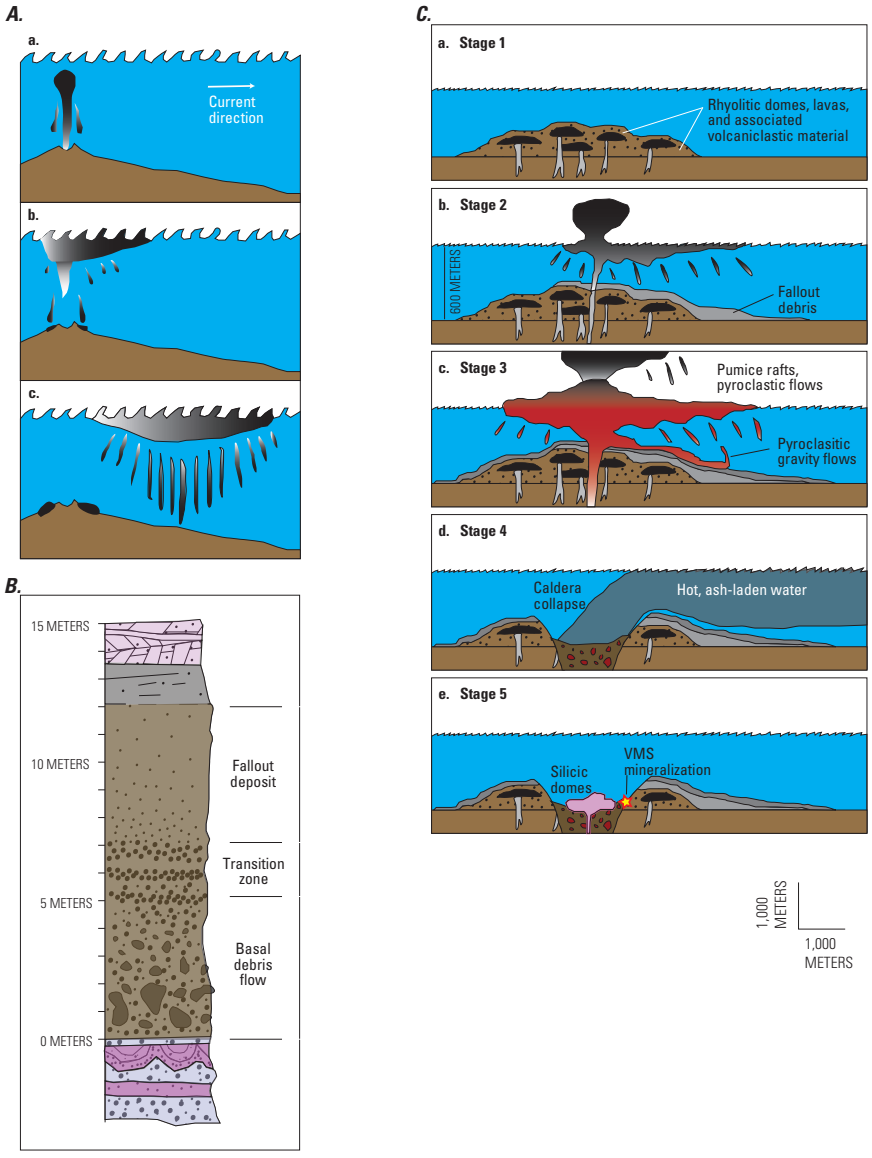

Figure 5–12. Products of explosive dominated submarine calderas in bimodal-felsic volcanic suite. *A*, Schematic representations of fallout from short-lived submarine eruption; arrow shows direction of current. (a) Particles with the highest terminal velocities fall from the margin of the rising eruption column and are deposited close to vent. (b) Eruption has ceased yet particles with lower terminal velocities begin to fall from base of expanding umbrella region. (c) The plume of fallout material drifts with the prevailing current off of the volcanic vent area; extensive fallout occurs from vestiges of laterally drifting umbrella region. From Cashman and Fiske (1991). *B*, Schematic stratigraphic section of a 12-m-thick sequence of pyroclastic material in the Japanese Shirahama Group that has three main facies and is interpreted as the product of a single submarine eruption. From Cashman and Fiske (1991). *C*, Stages in the development of the Myojin Knoll volcano and its caldera. (a) Stage 1. Rhyolitic domes (in black) and associated volcaniclastic deposits (random spot pattern) overlap to form an early volcano edifice. (b) Stage 2. Pre-caldera pumice erupts from summit of the summit, which had shoaled to 600 meters below sea level. The eruption column carries pumice to near sea level; however, most of the pumice sinks because of quick cooling and saturation of water and forms a thick sequence of fallout deposits that blanket older parts of the volcano. Larger pumice rises to the sea surface and slowly sinks away from the volcanic vent, resulting in deposits at the volcano that are somewhat pumice depleted. (c) Stage 3. Eruption continues and climaxes with the eruption column breaching the ocean surface. Huge volumes of floating pyroclastic rafts and pyroclastic flows are produced, resulting in the initial collapse of the caldera. (d) Stage 4. Caldera collapse and generation of hot ash-laden water. (e) Stage 5. Caldera begins to fill with post-caldera dome complexes emplaced on floor of the caldera; arrow points to the location of a volcanogenic massive sulfide deposit on the caldera wall. From Fiske and others (2001).

Siliciclastic-Felsic Volcanic Suite (Mature Epicontinental Margin Arcs and Back Arcs)

The siliciclastic-felsic association forms in mature epicontinental margin terranes and related back-arc settings (fig. 5-13A) (see Fig. 5-14A) (Franklin and others, 2005). About 80 percent of the strata are siliciclastic, the remainder being felsic volcaniclastic rocks with minor flows, domes, and subvolcanic intrusives. Mafic (alkaline to tholeiitic) flows and domes, sills, and volcaniclastic material can contribute up to about 10 percent of the total sequence (Franklin and others, 2005). Excellent examples of the siliciclastic-felsic assemblage are found in the Iberian Pyrite Belt in Spain and Portugal (Fig. 5-13) and the Bathurst district in Canada, as well as the Altai-Sayan region in Russia and Kazakhstan (fig. 5-14).

The Iberian Pyrite Belt hosts one of the largest concentrations of economic VMS deposits in volcano-sedimentary sequences of Upper Devonian to Lower Carboniferous age (Soriano and Marti, 1999). Volcanic rocks contribute only about 25 percent to the stratigraphic sequence but have greatly influenced mineralization. Rhyolitic pyroclastic and effusive deposits are intercalated with mudstone, which records a submarine, below-wave-base environment of deposition (fig. 5-13) (Rosa and others, 2008).

At the Neves Corvo deposit, volcanism began after a long period of volcanic quiescence. Several volcanic events record a 35-m.y. history of sedimentation interspersed with 3 major periods of volcanism spanning 22 m.y. (Rosa and others, 2008). The initial explosive volcanism generated at least two eruption-fed, thick, gravity flows of rhyolitic pumice-rich breccia, probably from multiple vents; an explosive origin is debatable (Soriano and Marti, 1999; Rosa and others, 2008). Lenses containing coarse fiamme (stretched and flattened pumice) in a laminated mudstone indicate that the pumice and mud particles were deposited at the same time. Sequences of fiamme, each ranging from 10 to 45 m in thickness, show no evidence for hot emplacement and, thus, deformation and flattening of the pumice is inferred to be diagenetic rather than hot welding and compaction (Rosa and others, 2008). A subsequent period of effusive, quench-fragmented rhyolitic volcanism from intra-basinal vents is intimately associated with and hosts VMS mineralization. These rhyolitic lavas range in thickness from about 250 m (presumably close to its source vent) to 85 m (at more distal locations). The lavas have coherent lobes and abundant rhyolitic hyaloclastites, a common submarine rhyolitic assemblage. A final volcanic event was explosive but minor compared to the earlier two events. In the Neves Corvo host succession, fourteen units are present: ten are volcanic and four are fine-grained sedimentary (Rosa and others, 2008).

The Rio Tinto area of the Iberian Pyrite Belt is a 1-km-thick volcano-sedimentary sequence, 80 percent of which is composed of high-level intrusions emplaced contemporaneously into wet mudstones (Boulter, 1993a, 1993b, 1996; Gibson and others, 1999). The intrusions grade upward from a 300-m-thick sequence of single and multiple doleritic sills into a 600-m-thick sequence of rhyolitic sills in the upper 600 m (see fig. 5-14A). The peperitic lobes contain fragments of mudstone that penetrated the sills when the sill margins fragmented upon emplacement into the wet unconsolidated sediment. Some of the upper rhyolite sills surfaced into the subaqueous environment and resulted in explosive fragmentation and generation of sediment-bearing hyaloclastites. These deposits then were resedimented in fault-controlled basins (Gibson and others, 1999).

Many VMS deposits throughout the Iberian Pyrite Belt typify the siliciclastic-felsic association with two distinct sedimentary facies. One facies is a siliciclastic-dominated assemblage of wacke, sandstone, siltstone, and locally iron formation or Fe-Mn-rich argillite. The second facies is a pelitic-dominated assemblage of argillite, carbonaceous argillite, siltstone, marl, and carbonate (Franklin and others, 2005) (fig. 5-13B). Volcanogenic massive sulfide deposits in these terranes may be enclosed within hundreds of meters of sedimentary or epiclastic materials.

The Bathurst mining camp, part of the Bathurst Supergroup, New Brunswick, Canada, provides another excellent example of the siliciclastic-felsic association involving world-class VMS deposits (fig. 5-14B). Large volumes of mafic and felsic volcanic rocks are interspersed with sediments formed in a tectonically complex back-arc basin setting (van Staal and others, 2003). At Bathurst, forty-five volcanic sediment-hosted VMS deposits formed in a sediment-covered, back-arc continental rift, which was intensely deformed and metamorphosed from subsequent multiple collisional events (Goodfellow and McCutcheon, 2003; Franklin and others, 2005). The Bathurst Supergroup is divided into five major sedimentary-volcanic sequences that formed in different parts of the back-arc basin. Each sequence has a bimodal-felsic to mafic phase in varying proportions with subvolcanic intrusions, which are associated with thinning of the crust during rifting (Goodfellow and McCutcheon, 2003; Rogers and others, 2003; Rogers and van Staal, 2003). Each sequence begins with eruptions of silicic flows and submarine epiclastic, volcaniclastic, and pyroclastic deposits that range from dacite to rhyolite and contain aphyric to crystal-rich tuffs, hyaloclastite, autobreccias, and subvolcanic rhyolitic cryptodomes (Goodfellow and others, 2003). These tectonically complex sequences most likely formed in different rift basin settings and were later subducted (possibly obducted) and then structurally juxtaposed during the Late Ordovician to Late Silurian (Goodfellow and others, 2003; McNicoll and others, 2003; van Staal and others, 2003). Felsic magmatism was followed by VMS mineralization and later emplacement of alkaline and tholeiitic basaltic lava flows and hyaloclastites; this change in magmatic composition was associated with continued back-arc rifting. The progression in composition in the mafic magmas from alkaline to tholeiitic may reflect the transformation from a back-arc basin into oceanic marginal sea (van Staal and others, 2003), which also was marked by the cessation of felsic magmatism and the deposition of maroon-colored pelagic mudstone, siltstone, and chert intercalated with flows of alkaline basalt (Goodfellow and

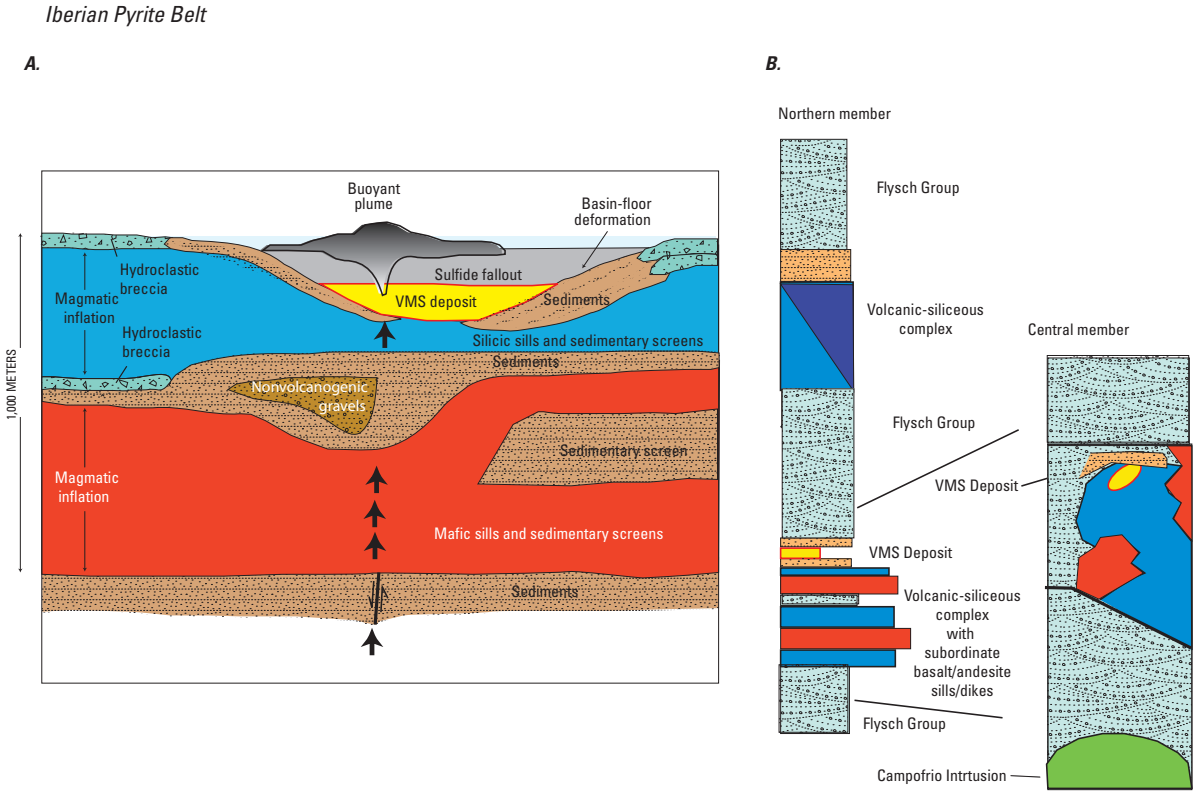

Figure 5–13. The Iberian Pyrite Belt, where volcanogenic massive sulfide mineralization has occurred in a siliciclastic-felsic suite, is shown in a schematic geologic cross section (*A*) and generalized stratigraphic sections (*B*). A, schematic cross section of the Rio Tinto mine showing the location of the volcanogenic massive sulfide deposit and sediment-sill complexes. After Boulter, 1993a. *B*, stratigraphic sections of the northern and central members of the Iberian Pyrite Belt. From Franklin and others (2005).

others, 2003). The textures and compositions of the sedimentary rocks indicate that the back-arc basins formed in varying water depths; some basins had shallow water submarine to subaerial environments whereas others were in much deeper marine environments (fig. 5-4*C*). Goodfellow and others (2003) note that Phanerozoic VMS deposits tend to be associated with sediments that formed under anoxic conditions and formed at times when ocean waters were rich in H_20.

The Devonian rift-related Altai-Sayan region in Kazakhstan and Russia is another excellent example of VMS deposition associated with siliciclastic-felsic facies. Here, the base and top of the rift sequence are marked by regional unconformities. Siliclastic sediments constitute about 80% of the strata with felsic volcaniclastic rocks with minor flows, domes, and intrusive rocks contributing up to about 25% of the strata. Similar to other siliciclastic-felsic facies, mafic rocks of tholeiitic and alkaline lava flows, sills, and volcaniclastic making up less than 10% of strata (Fig. 5-14C).

Siliciclastic-Mafic Volcanic Suite (Rifted Continental Margin, Intracontinental Rift, or Sedimented Oceanic Ridge)

The siliciclastic-mafic association forms in continental margin arcs and related back-arc settings (Franklin and others, 2005) (fig. 5-1 inset). Basalt and pelitic sediments are subequal, or pelite may dominate. The volcanic component is primarily shallow synvolcanic basaltic sills that may make up about 25 percent of the entire sequence. Felsic volcanic rocks, if present, contribute <5 percent of the total succession (Franklin and others, 2005) (fig. 5-15).

An excellent example of the siliciclastic-mafic suite is Windy Craggy (fig. 5-15). Pelitic host rocks of the Windy Craggy deposit formed in a mature back-arc basin. The presence of only minor tuff beds coupled with the absence of any coarse-grained turbiditic sediments suggest that sedimentation

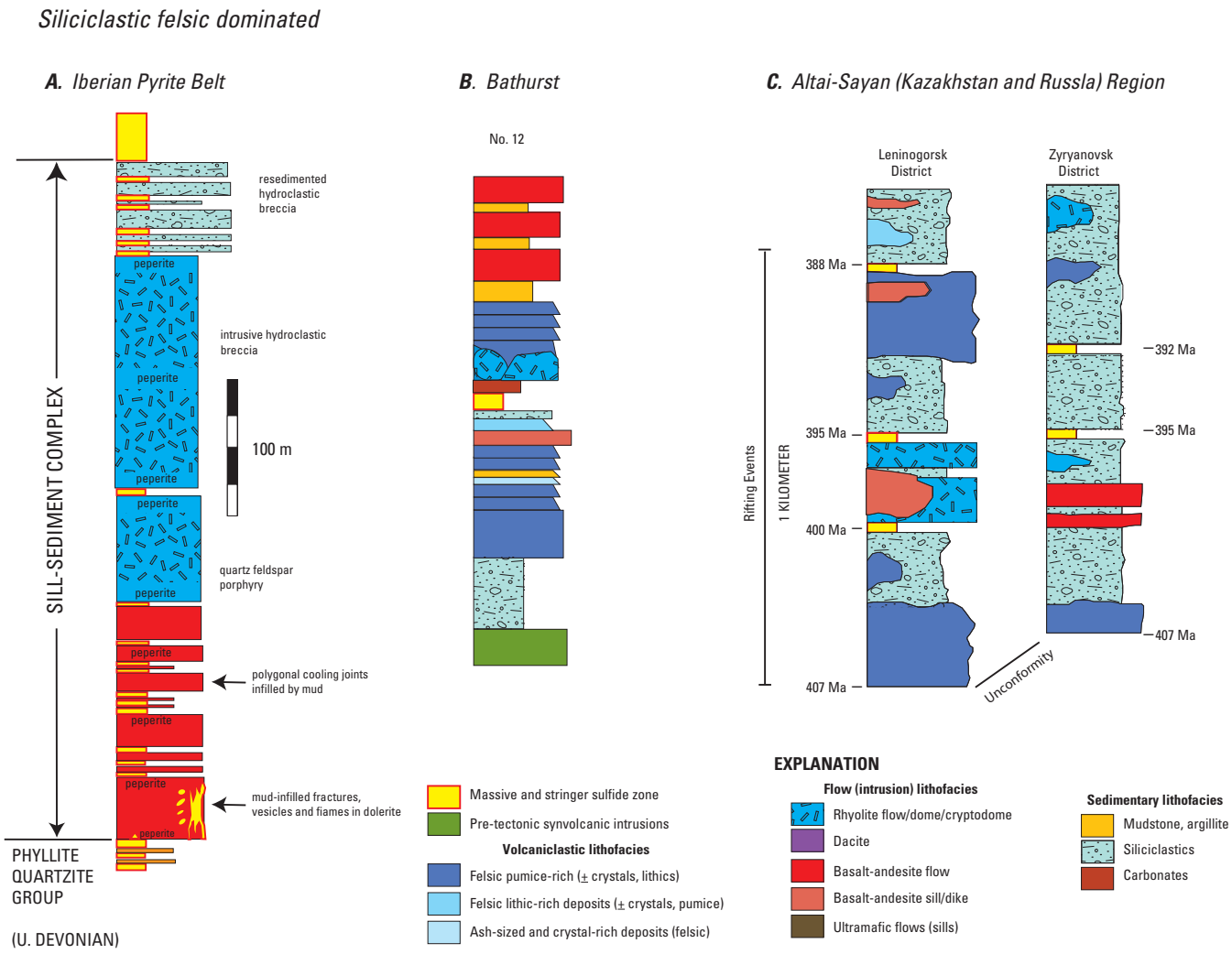

Figure 5–14. Composite stratigraphic sections for various areas hosting VMS mineralization in the siliciclastic-felsic dominated association. *A*. Generalized stratigraphic section through a sill-sediment complex in the Iberian Pyrite Belt. Note the abundance of peperite, polygonal cooling joints, and hydroclastic breccia indicative of the influential role of water and saturated sediments on emplacement of high-level intrusions. *B*. Generalized stratigraphic section at Bathurst no. 12. *C*. Generalized stratigraphic sections from the Altai-Sayan Region (Kazakhstan and Russia) showing the stratigraphic positions of significant VMS mineralization that are characteristic of siliciclastic-felsic dominated associations in the Leninogorsk and Zyryanovsk districts. From Frankin and others (2005).

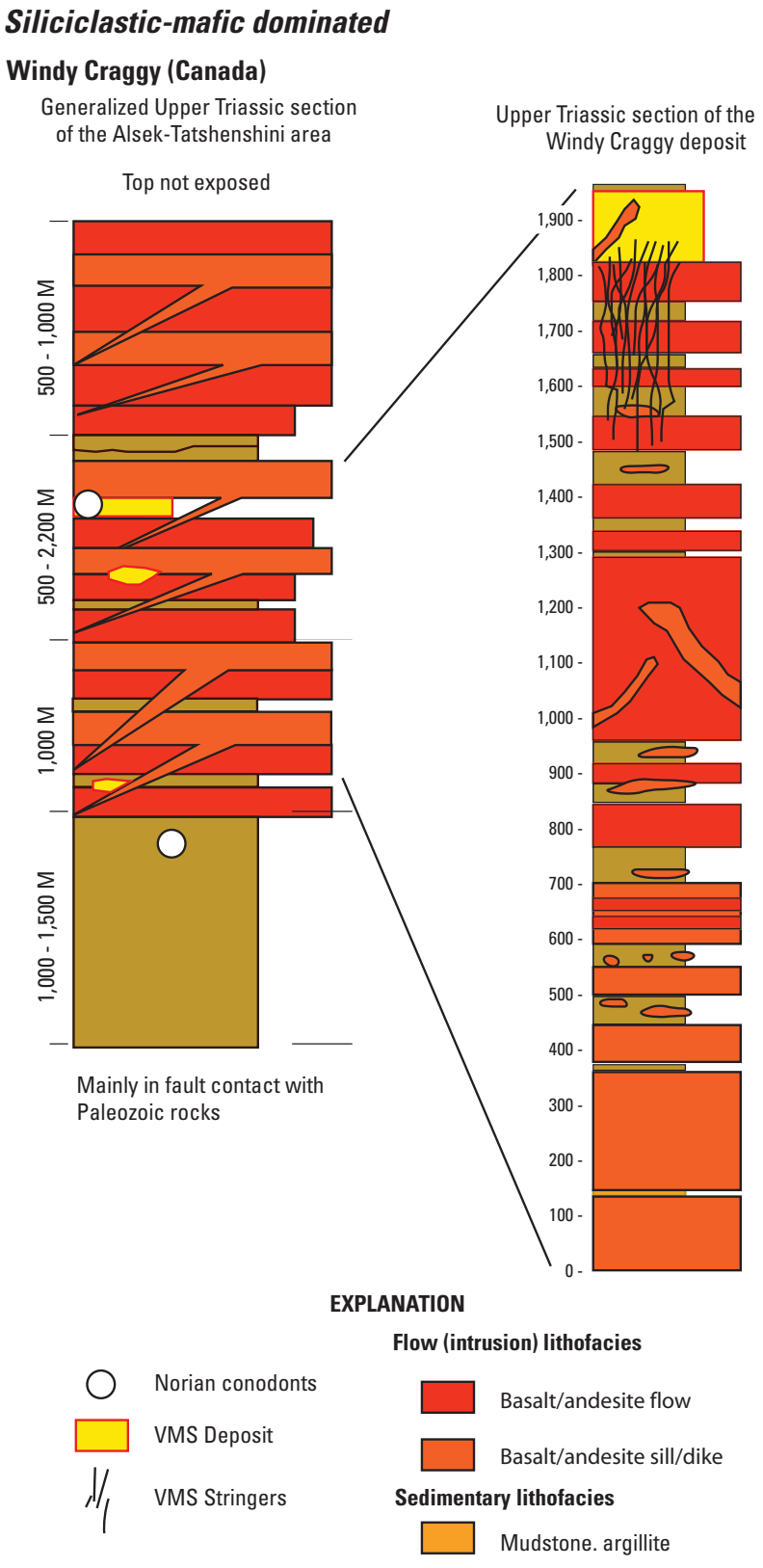

Figure 5–15. Generalized stratigraphic sections from the Windy Craggy (Canada) district, an example of VMS mineralization in siliciclastic-mafic dominated terranes. Note the absence of volcanic units in the lower parts of the generalized section. Modified from van Staal and others (2005) and Carvalho and others (1999). From Franklin and other (2005).

occurred far from a clastic source, for example, a subaerial island arc (Klein, 1975; Peter and Scott, 1999). Mafic lava flows and synvolcanic sills are interspersed with carbonaceous argillites that host the VMS mineralization (Franklin and others, 2005). Primary textures in the silicified basalts have been obliterated by a mosaic of interlocking microcrystalline quartz with minor clusters of fine-grained chlorite (Peter and Scott, 1999). Franklin and others (2005) envisage a very shallow volcanic center developed near the seafloor where numerous high-level basaltic dikes, sills, and cryptodomes were emplaced into unconsolidated carbonaceous argillite.

In the mature back-arc basin setting, igneous activity is primarily subvolcanic and is the driver for VMS mineralization, even though the associated mafic suite may amount to only about 25 percent of the total sequence. As Moore (1970) noted, the volume of magma associated with subvolcanic intrusions exceeds the volume of magma erupted as lava flows or pyroclastic material by several orders of magnitude. Mapping of dikes and sills is important in determining their proximity to source. By plotting their density, thickness, location, orientation, and composition, a facies architecture can be determined. These data reveal processes that were operating prior to and during volcanism and may define the area of most intense VMS mineralization where the areas of highest heat flow and cross-stratal permeability may occur (Gibson and others, 1999; Gibson, 2005). Dikes and sills represent the magmatic conduits for the eruptions and commonly occur on faults. Dikes and sills are commonly reactivated structures for repeated injections of magma and later act as conduits for hydrothermal fluids (Gibson and others, 1999).

The ascent and emplacement of magma in the near surface are controlled by the bulk density and hydrostatic pressure of the magma compared with the bulk density of the country rocks and lithostatic pressure (fig. 5-16). Magma denser than its host tends to remain in the subsurface and be intruded as sills and dikes below the level of neutral buoyancy rather than erupt as lavas at the surface (Walker, 1989). In subaqueous settings, such as in a mature back-arc basin, thick accumulations of saturated unconsolidated sediments, whose wet density is generally less than 2.0 (fig. 5-16) (Moore, 1962), act as a perfect host for the emplacement of denser sills and dikes. Magmas are unlikely to erupt as lava flows in this sediment-dominated basin environment (McBirney, 1963; McPhie and others, 1993). Thick sequences of unconsolidated pelitic sediments are intercalated with volcanic intrusives and co-genetic related rocks, such as peperites (McPhie and others, 1993). The level of neutral buoyancy controls whether the magma will be emplaced as an intrusive or extrusive.

Quenched compositions of dikes and sills are identical to the lavas they fed. Dike swarms are commonly identified by evidence of multiple intrusions into the same structure. Contacts of intrusions into wet unconsolidated sediments show that the intrusions have quenched, locally thin, chilled contacts defined by peperite (McPhie and others, 1993). Feeder dikes can be subdivided into four different categories based on the character of their margins and associated hyaloclastite. Yamagishi (1987, 1991) classifies apophyseal-type feeder dikes as those with bulbous or feeder-like protrusions into wet sediments; these break off into small concentric pillows. At the other end of the spectrum, massive feeder dikes are closely jointed and grade outward to angular fragment breccia and peperite (Yamagishi, 1987, 1991; McPhie and others, 1993). These are excellent conditions for VMS.

Subvolcanic Intrusions

Most volcanic-hosted massive sulfide districts form in proximal volcanic environments defined by vent to proximal facies volcanic sequences, with more than 75 percent of known deposits associated with felsic intrusive complexes (Franklin and others, 1981). In these settings, subvolcanic intrusions, representing the volcanic feeder system to the submarine volcanism, act as the thermal engine that drives hydrothermal convection cells that form VMS deposits on or near the seafloor (Galley, 2003). It is also inferred that shallow subvolcanic intrusions (2–5 km) may directly supply magmatic fluids and metals to the hydrothermal systems, particularly in the early stages of their development (Lydon, 1996; Yang and Scott, 1996; Hannington and others, 1999). Subvolcanic intrusions related to proximal facies volcanic sequences are one of the most important indicators of VMS potential (Franklin and others, 2005).

Subvolcanic intrusions can take four different forms representing different stages of magmatic activity and volcanism (fig. 5-17; Galley, 1996). The first is as large plutons or batholiths intruded 10–20 km below the seafloor, usually at or near the brittle-ductile transition zone in the crust (approximately the 450 °C isotherm) (A in fig. 5-17). These plutons are formed from primary melts from the mantle and (or) partial melts of the lower crust and represent lower magma chambers to the evolving volcanic system. However, such deep intrusions are unlikely to drive shallow hydrothermal convection because convection cells involving large amounts of seawater require relatively high permeability that can only be established within the zone of brittle deformation where open pore or fracture porosity can be maintained (Lydon, 1996).

The rise of magma batches from the lower magma chambers forms a second level of shallowly emplaced sills and stocks at depths generally less than 2–4 km (B in fig. 5-17). These intrusive phases tend to cluster asymmetrically below the eruptive centers in the comagmatic extrusive sequence. In most subvolcanic suites, the intrusive complexes are typically less than 2,000 m in width and commonly about 15–25 km in strike length (Franklin and others, 2005). The size of an intrusive complex is at least in part a function of the width, or diameter, of the volcanic subsidence structure under which it is emplaced (for example, Flavrian pluton, Noranda cauldron: Gibson and Watkinson, 1990; Beidelman Bay pluton, Sturgeon Lake caldera: Morton and others, 1991). In addition, the thickness of the intrusive complex appears to be directly related to the thickness of the overlying volcanic pile, although intrusion

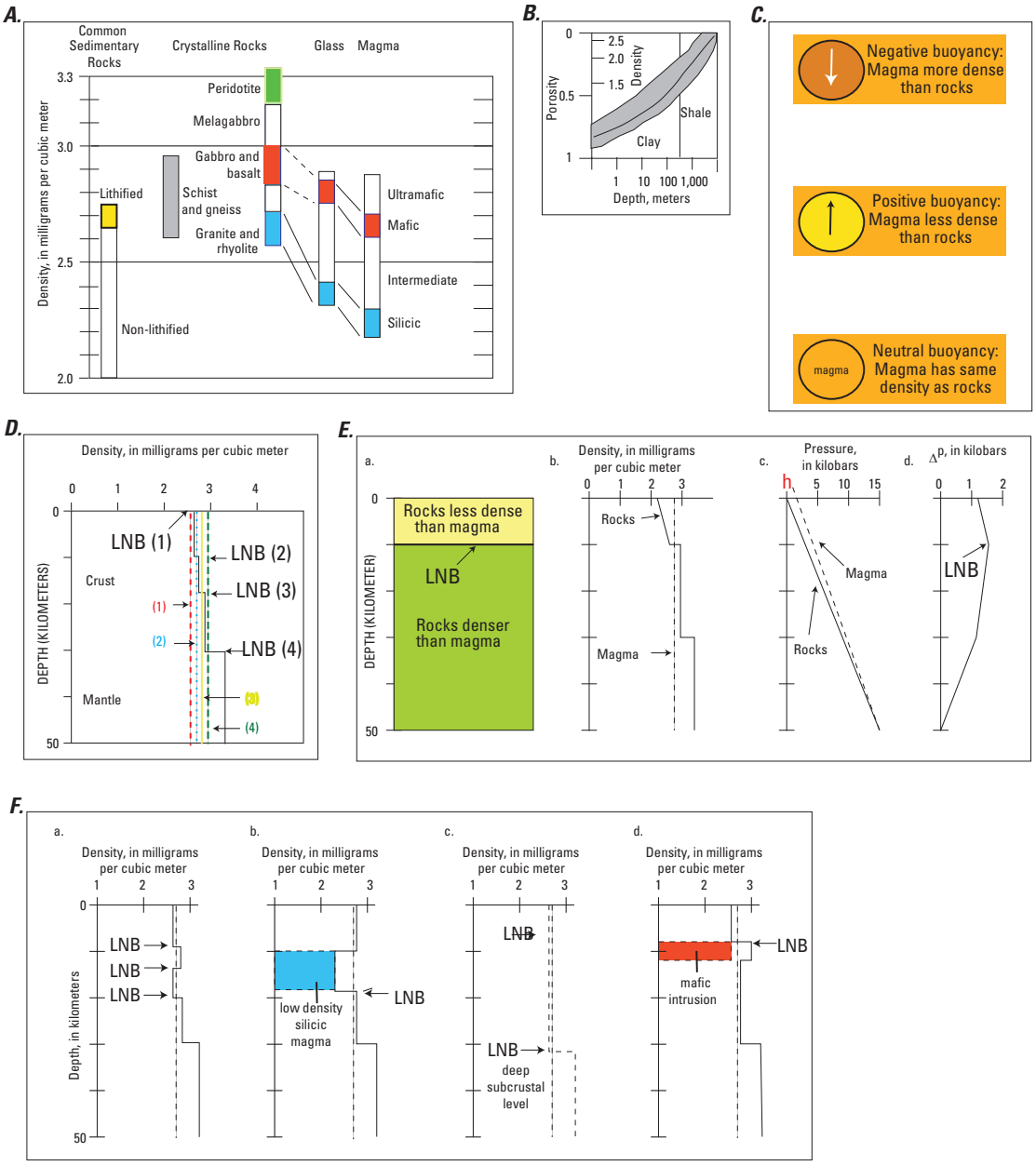

Figure 5–16. Physical parameters and controls on volcanism. *A*, Graph showing densities of common rock types and magmas of varying composition. *B*, Graph of porosity versus depth for young sediments; density increases and porosity decreases with increasing depth of burial. *C*, The net gravitational force (shown by arrow) exerted on magmas enclosed in less dense, denser, or equally dense rocks. *D*, Graph of the levels of neutral buoyancy (LNB) as a function of magma density for four different cases. *E*, Inferred behavior of mafic magma in a simple 2-layered crust. (a) Position of the idealized level of neutral buoyancy where intrusion is favored. (b) Graph of density versus depth profile for various crustal lithologies compared to a magma of uniform density. The cross-over point is the level of neutral buoyancy. (c) Graph of lithostatic pressure and magma hydrostatic pressure versus depth. Hydrostatic pressure is equal the lithostatic load pressure at an arbitrary 50 km depth. The difference (h) between the magma hydrostatic pressure and surface pressure determines the maximum height of h is the height to which hydrostatic pressure to which a volcano could be constructed and is usually reflected in the height of long-lasting lava lakes. (d) Difference between hydrostatic and lithostatic pressure, Dp, reaches a maximum value at the level of neutral buoyancy. *F*, Graphs of specific examples of the levels of neutral buoyancy. (a) Several levels of neutral buoyancy resulting from country rocks of varying density. (b) Neutral buoyancy at the base of a low-density silicic magma body. (c) Neutral buoyancy at a deep subcrustal level. (d) Neutral buoyancy at the top of a mafic intrusion. From Walker (1989).

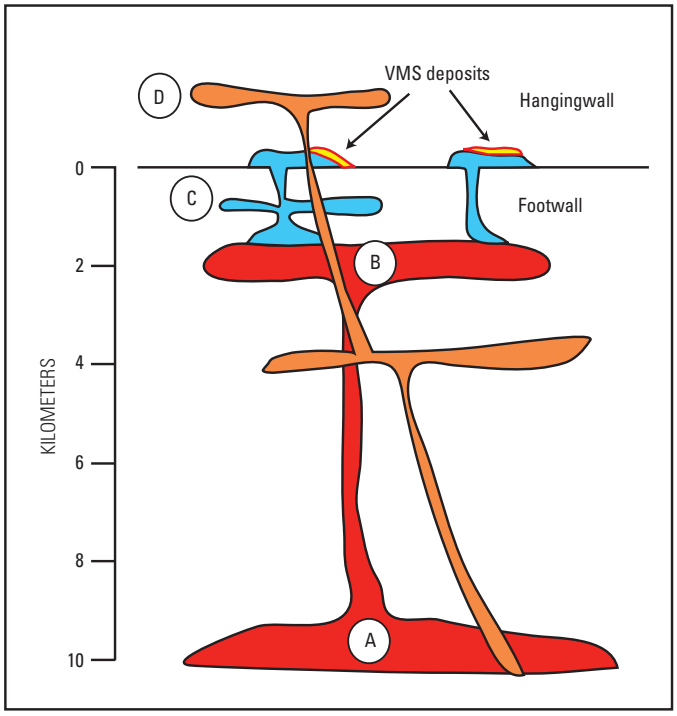

Figure 5–17. Schematic of a volcanic section hosting volcanogenic massive sulfide (VMS) showing relative positions of subvolcanic intrusions. *A*, Deep magma chamber with melts from mantle and/or lower crustal melting. *B*, High-level subvolcanic intrusive complex. *C*, Shallow sill-dike swarms feeding VMS-hosting rhyolites. *D*, Post-mineralization intrusions. After Galley (1996).

of post-VMS resurgent magmatic phases during hanging wall volcanic activity makes it difficult to quantify this relationship. Due to their shallow emplacement and composite nature (that is, long-lived), these intrusive complexes are often intimately associated with large-scale alteration systems and are proximal to massive sulfide horizons (Galley, 1996, 2003).

A third level of subvolcanic intrusion involves the largely vertical emplacement of dike swarms that are feeders to the overlying volcanic units (C in fig. 5-17). Often these dikes are localized along synvolcanic structures, such as caldera margins (Old Waite dike swarm, Noranda cauldron; Gibson and Watkinson, 1990) or spreading axes (sheeted dike swarms in ophiolites; Galley and Koski, 1999). In other cases they may form a series of sills and associated dikes such as the Powderhouse sill/dike swarm at Snow Lake, Canada (Bailes, 1988). These dike swarms are commonly characterized by a variety of compositions that can range from ultramafic to felsic, often representing a much wider variation than is present in either the host volcanic package or the underlying subvolcanic intrusions (Galley, 1996).

The fourth level of intrusions includes dikes and sills that represent feeders to the volcanic units in the hanging wall to the massive sulfide-bearing rocks. These dikes can cut the shallow intrusive complexes, footwall dike swarms, and the VMS deposits along long-lived synvolcanic structures. In some cases (for example, Chisel Lake deposit, Snow Lake), these crosscutting dikes are altered where they transect the deposit's footwall alteration zone and have altered margins well up into the hanging wall, indicating that they were intruded into a still-active subseafloor hydrothermal system (Galley and others, 1993). The recognition of discrete concentrations of sills and dikes within a volcanic package is important in identifying zones of long-lived synvolcanic extension along which VMS deposits can occur at several levels in the volcanic sequence.

Shallow level intrusive complexes emplaced in extensional regimes within oceanic arc environments (for example, nascent arc or primitive arc rifts) are characterized by low-alumina quartz diorite-tonalite-trondhjemite composition and are co-magmatic with the host volcanic strata (Lesher and others, 1986; Galley, 1996, 2003). These are the most common type of subvolcanic intrusive suites associated with clusters of VMS deposits, particularly in the Precambrian (>80 percent; Galley, 2003). Their high initial temperatures and relatively anhydrous composition allow the intrusions to rise rapidly to shallow crustal levels where an efficient transfer of heat from the magmas to the surrounding, fluid-rich volcanic pile results in convective hydrothermal fluid flow (Lydon, 1996). Well-described examples include the Archean Beidelman Bay intrusive complex, Sturgeon Lake caldera, Canada (Poulsen and Franklin, 1981; Morton and others, 1991); Archean Flavrian-Powell intrusion, Noranda cauldron, Canada (fig. 5-18) (Goldie, 1978; Gibson and Watkinson, 1990; Galley, 2003); and Paleoproterozoic Sneath Lake and Richard Lake intrusions, Snow Lake, Canada (Galley, 1996, 2003). In environments with continental crust (for example, epicontinental margin, continental-margin arc), intrusive complexes can include granodiorite, quartz monzonite, and granite (for example, Ordovician Bathurst camp, Canada: Whalen and others, 1998; Paleozoic Mount Read district: Large and others, 1996).

The interpretation that subvolcanic intrusions are the primary heat engines responsible for hydrothermal systems is supported by a number of observations (Galley, 2003; Franklin and others, 2005) including:

1. a close spatial relationship between subvolcanic intrusions and clusters of VMS deposits (fig. 5-18);

2. volcanic strata for several thousand meters above the intrusions containing a stratified, district-scale semi-conformable alteration zone defined by distinctive metasomatic mineral assemblages controlled in extent by the strike length of the underlying intrusion;

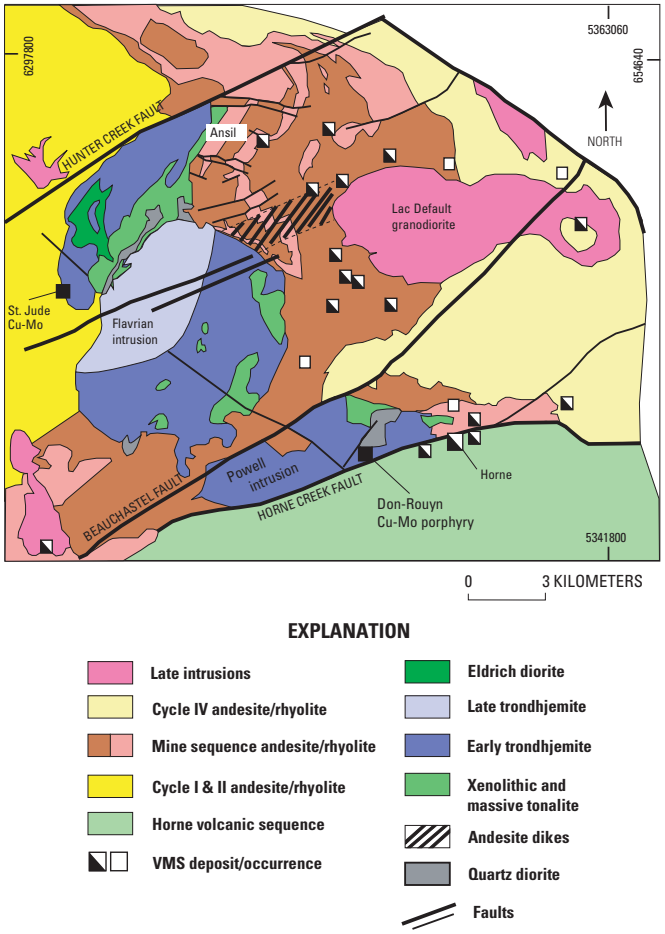

Figure 5–18. Geologic map of the Archean Noranda volcanogenic massive sulfide (VMS) camp showing the VMS deposits underlain by the Flavrian-Powell subvolcanic intrusive complex. After Galley (2003). [Cu, copper; Mo, molybdenum].

3. in some, the most intense alteration lying directly above and within the margin of the subvolcanic intrusions;

4. an apparent positive relationship between the aggregate massive sulfide tonnage in the host VMS district and the size of the associated subvolcanic intrusion for intrusions less than 60 km^2; and

5. low whole-rock oxygen isotope values relative to unaltered rocks, providing quantitative evidence that the subvolcanic intrusions have reacted with hot, evolved seawater.

The identification of a subvolcanic intrusive complex is important for determining VMS potential and for defining exploration targets. Because the intrusive complexes are typically much larger than their comagmatic rhyolites that host VMS deposits, they provide a much larger target to identify prospective volcanic sequences. However, identifying the intrusions can be difficult, particularly in orogenic belts where younger volcanic and tectonic-related intrusions occur, and the effects of deformation and metamorphism can be intense.

Three features of subvolcanic intrusive high-level intrusions are that they form the cores of early fold structures in deformed terranes, are grossly conformable with the host strata, and seldom have significant contact metamorphic haloes. Although sill-like in their overall morphology, these complexes typically consist of a series of stocks, sills, and dike swarms that were emplaced at about the same stratigraphic level within the volcanic sequence. They are commonly zoned, with more mafic hornblende-rich gabbroic, or dioritic, phases successively intruded by more felsic tonalite, trondhjemite, and granite stocks, sills, and dikes (fig. 5-18). Contacts between intrusive phases range from sharp to diffuse and transitional and provide evidence that intrusion of more felsic phases often occurred before full crystallization of the more mafic magma (Galley, 2003). Late-stage felsic intrusive phases (trondhjemites) also are often coarser grained than the early phases (Galley, 2003). This textural change may be an indication of a deeper emplacement depth and slower cooling for the felsic phases, perhaps as a result of thickening of the volcanic pile during the emplacement of the intrusive complex.

Evidence for rapid cooling of particularly the early intrusions through contact with a convecting external fluid is provided by the presence of a variety of disequilibrium textures such as complex compositional zonation of feldpars in mafic phases, myrmekitic textures, development of granophyre, acicular growth of pyroxene and amphibole, and the development of miarolitic cavities in the more felsic phases (Poulsen and Franklin, 1981; Galley, 2003). In addition, the presence of pegmatitic coronas around some xenoliths, abundant miarolitic cavities and (or) an increased volume of magmatic/hydrothermal alteration characterized by replacement and infilling by epidote, actinolite, quartz, albite, magnetite, and subordinate sulfide minerals provide evidence for the introduction into the cooling intrusions of seawater from external sources as well as possible devolitization of the rapidly cooled magmas (Franklin and others, 2005). Various geochemical approaches can also help in the discrimination of synvolcanic intrusions from later tectonic and post-tectonic intrusions (Galley, 1996; Gaboury, 2006).

Summary and Conclusions

Volcanogenic massive sulfide mineralization occurs in a broad variety of submarine volcano-tectonic settings. Each setting has a distinctive suite of volcanically associated rocks that reflect a variety of volcanic, intrusive, and (or) sedimentalogical processes. Volcanogenic massive sulfide mineralization has five broad stratigraphic associations each with a distinctive volcanic lithofacies that falls into two broad subdivisions: (1) lithofacies developed by extrusive processes, as observed within the mafic-ultramafic association, the bimodal mafic association, and the bimodal felsic association; and

(2) lithofacies developed by primary and redeposited syn-eruptive pyroclastic deposits and subvolcanic intrusions, as observed within the siliciclastic-felsic association and the siliclastic-mafic association. The differences between the two may reflect deposition and emplacement in deep marine settings for the former subdivision versus shallower water environments for the latter subdivision. In addition, a hierarchy of architectural and lithofacies complexity ranges from the relatively simple siliciclastic-mafic association through the more complex mafic-ultramafic association to the highly complicated bimodal-mafic, bimodal-felsic, and siliciclastic-felsic associations (Gibson and others, 1999; Gibson, 2005). This hierarchy reflects the relative complexities of volcanic processes.

The application of physical volcanology is critical in characterizing terrane and interpretating the volcanic processes that accompany formation of VMS deposits. Thus, the key to understanding the dynamic environment of volcanism which localized VMS mineralization lies in the identification of volcanic lithofacies. A series of mafic pillow lavas overlying sheeted dikes above layered gabbro and mantle peridotite occur typically at mid-ocean ridge and mature back-arc environs. The ultramafic suite of rocks may form in slow to ultra-slow spreading environments where the classic penrose crustal successions are absent. However, back-arc basins may never develop spreading ridges, so that open-ocean crustal architecture does not develop. In this case, VMS mineralization here is hosted by pillow lavas. In incipient-rifted intraoceanic arcs, a bimodal-mafic assemblage records volcanism dominated by large subaqueous shield volcanoes with later developed summit calderas filled with silicic lavas; these also are found on the arc front (for example, Izu-Bonin arc; Fiske and others, 2001). Here, mafic pillow lavas overlie felsic domes or subvolcanic intrusions: rhyolitic lobe-hyaloclastite flows are found interbedded with the mafic pillow lavas. In contrast, incipient-rifted continental margin arc and back-arc settings produce a bimodal-felsic suite of primarily volcanic rocks dominated by explosive felsic volcaniclastic deposits intercalated with effusive lava flows. Mafic volcanism here is a subordinate component, and contributions from terrigenous sediments are minor but present. Mature epicontinental margin arcs and back arcs produce siliciclastic-felsic suite assemblages which reflect a prolonged history of sedimentation interspersed with silicic volcanism; mafic volcanism is rare and limited. Volcanic products include abundant pyroclastic flow and fall deposits, coarse turbidite deposits, sills, and subvolcanic intrusions. In rifted continental margin or intracontinental rift or sedimented oceanic ridges settings, the siliciclastic-mafic suite of rocks is dominated by fine-grained mudstones and argillites into which were intruded basaltic sills. These are simple subvolcanic settings but are host to some of the largest VMS deposits in the world. Each volcanic terrane produces a specific suite of lithofacies dependent on the tectonic setting.

Key elements in evaluating the prospectivity of ancient volcanic successions and VMS deposits appear to be deep-water sediments and lavas or shallow intrusions in an extensional basin setting. While many explosive submarine calderas are host to VMS deposits, extensive VMS mineralization also occurs in autoclastic breccias and hyaloclastites that formed non-explosively.

References Cited

Allen, R.L., 1988, False pyroclastic textures in altered silicic lavas, with implications for volcanic-associated mineralization: Economic Geology, v. 83, p. 1424–1446.

Barrie, C.T., and Hannington, M.D., 1999, Classification of volcanic-associated massive sulfide deposits based on host-rock composition, *in* Barrie, C.T., and Hannington, M.D., eds., Volcanic-associated massive sulfide deposits—Processes and examples in modern and ancient settings: Reviews in Economic Geology, v. 8. p. 1–11.

Bleeker, W., and Parrish, R.R., 1996, Stratigraphy and U-Pb zircon geochronology of Kidd Creek—Implications for the formation of giant volcanogenic massive sulfide deposits and the tectonic history of the Abitibi greenstone belt: Canadian Journal of Earth Sciences, v. 33, p. 1213–1321.

Bloomer, S.H., Stern, R.J., and Smoot, N.C., 1989, Physical volcanology of the submarine Mariana and Volcano Arcs: Bulletin of Volcanology, v. 51, p. 210–224.

Boulter, C.A., 1993a, Comparison of Rio Tinto, Spain, and Guaymas Basin, Gulf of California—An explanation of a supergiant massive sulfide deposit in an ancient sill-sediment complex: Geology, v. 21, no. 9, p. 801–804.

Boulter, C.A., 1993b, High-level peperitic sills at Rio Tinto, Spain—Implications for stratigraphy and mineralization: London, Institution of Mining and Metallurgy, Transactions, v. 102, p. B30–B38.

Boulter, C.A., 1996, Extensional tectonics and magmatism as drivers of convection leading to Iberian Pyrite Belt massive sulphide deposits?: Journal of the Geological Society, v. 153, no. 2, p. 181–184.

Burnham, C.W., 1983, Deep submarine pyroclastic eruptions: Economic Geology Monograph 5, p. 142–148.

Busby, C., 2005, Possible distinguishing characteristics of very deepwater explosive and effusive silicic volcanism: Geology, v. 33, p. 845–848.

Busby, C.J., Kessel, L., Schulz, K.J., Foose, M.P., and Slack, J.F., 2003, Volcanic setting of the Ordovician Bald Mountain massive sulfide deposit, northern Maine: Economic Geology Monograph 11, p. 219–244.

Carvalho, D., Barriga, F.J.A.S., and Munha, J., 1999, Bimodal siliciclastic systems—The case of the Iberian Pyrite Belt, *in* Barrie, C.T., and Hannington, M.D., eds., Volcanic-associated massive sulfide deposits—Processes and examples in modern and ancient settings: Reviews in Economic Geology, v. 8, p. 375–408.

Cas, R.A.F., 1992, Submarine volcanism—Eruption styles, products, and relevance to understanding the host-rock successions to volcanic-hosted massive sulfide deposits: Economic Geology, v. 87, p. 511–541.

Cas, R.A.F., and Wright, J.V., 1988, Volcanic successions—Modern and ancient. A geological approach to processes, products and successions: London, Unwin-Hyman, 528 p.

Cashman, K.V., Chadwick, B., Fiske, R.S., and Deardorff, N., 2009, A comparison of eruption mechanisms in subaerial and submarine arc environments [abs.]: EOS, Transactions, American Geophysical Union, v. 90, no. 52, Fall meeting supplement, abstract V44B-01, p. 394.

Cashman, K.V., and Fiske, R.S., 1991, Fallout of pyroclastic debris from submarine volcanic eruptions: Science, v. 253, no. 5017, p. 275–280.

Chadwick, B., Dziak, R.P., Baker, E., Cashman, K.V., Embley, R.W., Ferrini, V., de Ronde, C.E., Butterfield, D.A., Deardorff, N., Haxel, J.H., Matsumoto, H., Fowler, M.J., Walker, S.L., Bobbitt, A.M., and Merle, S.G., 2009, Continuous, long-term, cyclic, varied eruptive activity observed at NW Rota-1 submarine volcano, Mariana Arc [abs.]: EOS, Transactions, American Geophysical Union, v. 90, no. 52, Fall meeting supplement, abstract V44B-03, p. 394.

Chadwick, W.W., Jr., Cashman, K.V., Embley, R.W., Matsumoto, H., Dziak, R.P., de Ronde, C.E.J., Lau, T.K., Deardorff, N.D., and Merle, S.G., 2008, Direct video and hydrophone observations of submarine explosive eruptions at NW Rota-1 volcano, Mariana arc: Journal of Geophysical Research, v. 113, B08S10, 23 p., doi:10.1029/2007JB005215.

Clague, D.A., Paduan, J.B., and Davis, A.S., 2009, Widespread strombolian eruptions of mid-ocean ridge basalt: Journal of Volcanology and Geothermal Research, v. 180, p. 171–188.

Cousineau, P., and Dimroth, E., 1982, Interpretation of the relations between massive, pillowed and brecciated facies in an Archean submarine andesite volcano—Amulet Andesite, Rouyn-Noranda, Canada: Journal of Volcanology and Geothermal Research, v. 13, p. 83–102.

de Rosen-Spense, A.P., Provost, G., Dimroth, E., Gochnauer, K., and Owen, V., 1980, Archean subaqueous felsic flows, Rouyn-Noranda, Quebec, Canada and their Quaternary equivalents: Precambrian Research, v. 12, p. 43–77.

Dimroth, E., Cousineau, P., Leduc, M. and Sanschagrin, Y., 1978, Structure and organization of Archean subaqueous basalt flows, Rouyn-Noranda area, Quebec, Canada: Canadian Journal of Earth Sciences, v. 15, p. 902–918.

Dimroth, E., Imreh, L., Cousineau, P., Leduc, M., and Sanschagrin, Y., 1985, Paleogeographic analysis of mafic submarine flows and its use in the exploration for massive sulfide deposits: Geological Society of Canada, Special Paper 28, p. 202–222.

Embley, R.W., Baker, E.T., Chadwick, W.W., Jr., Lupton, J.E., Resing, J.A., Massoth, G.J., and Nakamura, K., 2004, Explorations of Mariana arc volcanoes reveal new hydrothermal systems: EOS, Transactions, American Geophysical Union, v. 85, no. 4, p. 37–40.

Ewart, A., and Hawkesworth, C.J., 1987, The Pliocene-Recent Tonga-Kermadec arc lavas—Interpretation of new isotopic and rare earth data in terms of a depleted mantle source model: Journal of Petrology, v. 28, p. 495–530.

Fisher, R.V., Heiken, G., and Hulen, J.B., 1997, Volcanoes—Crucibles of change: New Jersey, Princeton University Press, 317 p.

Fisher, R.V., and Schmincke, H.U., 1984, Pyroclastic rocks: Berlin, Springer-Verlag, 472 p.

Fiske, R.S., Naka, J., Iizasa, K., Yuasa, M., and Klaus, A., 2001, Submarine silicic caldera at the front of the Izu-Bonin Arc, Japan—Voluminous seafloor eruptions of rhyolite pumice: Geological Society of America Bulletin, v. 113, no. 7, p. 813–824.

Franklin, J.M., 1996, Volcanic-associated massive sulphide base metals, *in* Eckstrand, O.R., Sinclair, W.D., and Thorpe, R.I., eds., Geology of Canadian mineral deposit types: Geological Survey of Canada, Geology of Canada no.8; Geological Survey of America, Decade of North American Geology v. P1, p. 158–183.

Franklin, J.M., Gibson, H.L., Jonasson, I.R., and Galley, A.G., 2005, Volcanogenic massive sulfide deposits, *in* Hedenquist, J.W., Thompson, J.F.H., Goldfarb, R.J., and Richards, J.P., eds., Economic Geology 100th anniversary volume, 1905–2005: Littleton, Colo., Society of Economic Geologists, p. 523–560.

Franklin, J.M., Lydon, J.M., and Sangster, D.F., 1981, Volcanic-associated massive sulfide deposits, *in* Skinner, B.J., ed., Economic Geology 75th anniversary volume, 1905–1980: Littleton, Colo., Economic Geology Publishing Company, p. 485–627.

Fridleifsson, I.B., Furnes, H., and Atkins, F.B., 1982, Subglacial volcanic—On the control of magma chemistry on pillow dimensions: Journal of Volcanology and Geothermal Research, v. 13, p. 103–117.

Furnes, H., Fridleifsson, I.B., and Atkins, F.B., 1980, Subglacial volcanics—On the formation of acid hyaloclastites: Journal of Volcanology and Geothermal Research, v. 8, p. 95–110.

Gaboury, D., 2006, Geochemical approaches in the discrimination of synvolcanic intrusions as a guide for volcanogenic base metal exploration—An example from the Abitibi belt, Canada: Applied Earth Sciences—Transactions of the Institution of Mining and Metallurgy section B, v. 115, p. 71–79.

Galley, A.G., 1996, Geochemical characteristics of subvolcanic intrusions associated with Precambrian massive sulfide deposits, *in* Wyman, D.A., ed., Trace element geochemistry of volcanic rocks—Applications for massive sulfide exploration: Geological Association of Canada, Short Course Notes, v. 12, p. 239–278.

Galley, A.G., 2003, Composite synvolcanic intrusions associated with Precambrian VMS-related hydrothermal systems: Mineralium Deposita, v. 38, p. 443–473.

Galley, A.G., Bailes, A.H., and Kitzler, G., 1993, Geological setting and hydrothermal evolution of the Chisel Lake and North Chisel Zn-Pb-Ag-Au massive sulphide deposit, Snow Lake, Manitoba: Exploration and Mining Geology, v. 2, p. 271–295.

Galley, A.G., Hannington, M.D., and Jonasson, I.R., 2007, Volcanogenic massive sulphide deposits, *in* Goodfellow, W.D., ed., Mineral deposits of Canada—A synthesis of major deposit-types, district metallogeny, the evolution of geological provinces, and exploration methods: Geological Association of Canada, Mineral Deposits Division, Special Publication 5, p. 141–161.

Galley, A.G., and Koski, R.A., 1999, Setting and characteristics of ophiolite-hosted massive sulfide deposits: Reviews in Economic Geology, v. 8, p. 445–473.

Gibson, H.L., 2005, Volcano-hosted ore deposits, *in* Marti, J., and Ernst, G.G.J., eds., Volcanoes and the environment: New York, Cambridge University Press, p. 333–386.

Gibson, H.L., and Galley, A.G., 2007, Volcanogenic massive sulphide deposits of the Archean, Noranda District, Quebec, *in* Goodfellow, W.D., ed., Mineral deposits of Canada—A synthesis of major deposit-types, district metallogeny, the evolution of geological provinces, and exploration methods: Geological Association of Canada, Mineral Deposits Division, Special Publication 5, p. 533–552.

Gibson, H.L., and Gamble, A.P.D., 2000, A reconstruction of the volcanic environment hosting Archean seafloor and subseafloor VMS mineralization at the Potter Mine, Munro Township, Ontario, Canada, *in* Gemmel, J.B., and Pongratz, J., eds., Volcanic environments and massive sulfide deposits: University of Tasmania, Australian Research Council, Center of Excellence in Ore Deposits (CODES) Special Publication 3, p. 65–66.

Gibson, H.L., Morton, R.L., and Hudak, G., 1999, Submarine volcanic processes, deposits, and environments favorable for the location of volcanic-associated massive sulfide deposits, *in* Barrie, C.T., and Hannington, M.D., eds., Volcanic-associated massive sulfide deposits—Processes and examples in modern and ancient settings: Reviews in Economic Geology, v. 8, p. 13–51.

Gibson, H.L., and Watkinson, D.H., 1990, Volcanogenic massive sulphide deposits of the Noranda cauldron and shield volcano, Quebec, *in* Rive, M., Verpaelst, P., Gagnon, Y., Lulin, J.M., Riverin, G., and Simard, A., eds., The northwestern Quebec polymetallic belt—A summary of 60 years of mining exploration: Canadian Institute of Mining and Metallurgy Transactions special volume, p. 119–132.

Goldie, R.J., 1978, Magma mixing in the Flavrian pluton, Noranda area, Quebec: Canadian Journal of Earth Sciences, v. 15, p. 132–144.

Goodfellow, W.D., and McCutcheon, S.R., 2003, Geological and genetic attributes of volcanic-associated massive sulfide deposits of the Bathurst mining camp, northern New Brunswick—A synthesis, *in* Goodfellow, W.D., McCutcheon, S.R., and Peter, J.M., eds., Massive sulfide deposits of the Bathurst mining camp, New Brunswick, and northern Maine: Economic Geology Monograph 11, p. 245–301.

Goodfellow, W.D., McCutcheon, S.R., and Peter, J.M., 2003, Introduction and summary of findings, *in* Goodfellow, W.D., McCutcheon, S.R., and Peter, J.M., eds., Massive sulfide deposits of the Bathurst mining camp, New Brunswick, and northern Maine: Economic Geology Monograph 11, p. 1–16.

Goto, Y., and McPhie, J., 2004, Morphology and propagation styles of Miocene submarine basanite lava at Stanley, northwestern Tasmania, Australia: Journal of Volcanology and Geothermal Research, v. 130, p. 307–328.

Hannington, M.D., Poulsen, K.H., Thompson, J.F.H., and Sillitoe, R.H., 1999, Volcanogenic gold in the massive sulfide environment, *in* Barrie, C.T., and Hannington, M.D., eds., Volcanic-associated massive sulfide deposits—Processes and examples in modern and ancient settings: Reviews in Economic Geology, v. 8, p. 325–356.

Hargreaves, R., and Ayres, L.D., 1979, Morphology of Archean metabasalt flows, Utik Lake, Manitoba: Canadian Journal of Earth Sciences, v. 16, p. 1452–1466.

Harper, G.D., 1984, The Josephine Ophiolite: Geological Society of America Bulletin, v. 95, p. 1009–1026.

Head, J.W., III, and Wilson, Lionel, 2003, Deep submarine pyroclastic eruptions—Theory and predicted landforms and deposits: Journal of Volcanology and Geothermal Research, v. 121, p. 155–193.

Huppert, H.E., and Sparks, S.J., 1985, Komatiites I—Eruption and flow: Journal of Petrology, v. 26, p. 694–725.

Kato, Y., 1987, Woody pumice generated with submarine eruption: Geological Society of Japan Journal, v. 93, p. 11–20.

Kessel, L.G., and Busby, C.J., 2003, Analysis of VHMS-hosting ignimbrites erupted at bathyal water depths (Ordovician Bald Mountain sequence, northern Maine), *in* White, J.D.L., Smelie, J.L., and Clague, D.A., eds., Explosive subaqueous volcanism: American Geophysical Union, Geophysical Monograph 140, p. 361–379.

Klein, G., 1975, Depositional facies of Leg 30 DSDP sediment cores, *in* Andrews, J.E., and Packham, G., eds., Initial reports of the Deep Sea Drilling Project: Washington, D.C., U.S. Government Printing Office, p. 423–442.

Kokelaar, P., 1986, Magma-water interactions in subaqueous and emergent basaltic volcanism: Bulletin of Volcanology, v. 48, no. 5, p. 275–289.

Large, R.R., Doyle, M., Raymond, O., Cooke, D., Jones, A., and Heasman, L., 1996, Evaluation of the role of Cambrian granites in the genesis of world class VMS deposits in Tasmania: Ore Geology Reviews, v. 10, p. 215–230.

Leat, P.T., and Larter, R.D., 2003, Intra-oceanic subduction systems—Introduction, *in* Larter, R.D., and Leat, P.T., eds., Intra-oceanic subduction systems—Tectonic and magmatic processes: Geological Society Special Publication 219, p. 1–18.

Lesher, C.M., Goodwin, A.M., Campbell, I.H., and Gorton, M.P., 1986, Trace-element geochemistry of ore-associated and barren, felsic metavolcanic rocks in the Superior Province, Canada: Canadian Journal of Earth Sciences, v. 23, no. 2, p. 222–237.

Lydon, J.W., 1996, Characteristics of volcanogenic massive sulfide deposits—Interpretations in terms of hydrothermal convection systems and magmatic hydrothermal systems: Instituto Tecnologico Geominero de Espana, Boletin Geologico y Minero, v. 107, no. 3–4, p. 15–64.

Mastin, L.G., and Witter, J.B., 2000, The hazards of eruptions through lakes and seawater: Journal of Volcanology and Geothermal Research, v. 97, p. 195–214.

McBirney, A.R., 1963, Factors governing the nature of submarine volcanism: Bulletin of Volcanology, v. 26, p. 455–469.

McNicoll, V.J., Whalen, J.B., and Stern, R.A., 2003, U-Pb geochronology of Ordovician plutonism, Bathurst mining camp, New Brunswick, *in* Goodfellow, W.D., McCutcheon, S.R., and Peter, J.M., eds., Massive sulfide deposits of the Bathurst mining camp, New Brunswick, and northern Maine: Economic Geology Monograph 11, p. 203–218.

McPhie, J., and Allen, R.L., 1992, Facies architecture of mineralized submarine volcanic sequences—Cambrian Mount Read volcanics, western Tasmania: Economic Geology, v. 87, no. 3, p. 587–596.

McPhie, J., Doyle, M., and Allen, R.L., 1993,Volcanic textures—A guide to the interpretation of textures in volcanic rocks: Hobart, Tasmania, University of Tasmania, Centre for Ore Deposit and Exploration Studies, 198 p.

Moore, D.G., 1962, Bearing strength and other physical properties of some shallow and deep-sea sediments from the North Pacific: Geological Society of America Bulletin, v. 73, p. 1163–1166.

Moore, J.G., 1970, Relationship between subsidence and volcanic load, Hawaii: Bulletin of Volcanology, v. 34, p. 526–576.

Moore, J.G., 1975, Mechanism of formation of pillow lava: American Scientist, v. 63, p. 269–277.

Morton, R.L., Walker, J.S., Hudak, G.J., and Franklin, J.M., 1991, The early development of an Archean submarine caldera complex with emphasis on the Mattabi ash-flow tuff and its relationship to the Mattabi massive sulfide deposit: Economic Geology, v. 86, p. 1002–1011.

Mosier, D.L., Berger, V.I., and Singer, D.A., 2009, Volcanogenic massive sulfide deposits of the world; database and grade and tonnage models: U.S. Geological Survey Open-File Report 2009–1034, 46 p. (Also available at http://pubs.usgs.gov/of/2009/1034/.)

Mueller, W.U., Stix, J.B., White, J.D.L., Corcoran, P.L., Lafrance, B., and Daigneault, R., 2008, Characterisation of Archean subaqueous calderas in Canada—Physical volcanology, carbonate-rich hydrothermal alteration and a new exploration model, *in* Gottsmann, J., and Marti, J., eds., Caldera volcanism—Analysis, modeling, and response: Developments in Volcanology, v. 10, p. 181–232.

Mueller, W.U., Stix, J., Corcoran, P.L., and Daigneault, R., 2009, Subaqueous calderas in the Archean Abitibi greenstone belt—An overview and new ideas: Ore Geology Reviews, v. 35, p. 4–46.

Pecover, R.S., Buchanan, D.J., and Ashby, D.E., 1973, Fuel-coolant interaction in submarine volcanism: Nature, v. 245, p. 307–308.

Peter, J.M., and Scott, S.D., 1999, Windy Craggy, northwestern British Columbia—The world's largest Besshi-type deposit, *in* Barrie, C.T., and Hannington, M.D., eds., Volcanic-associated massive sulfide deposits—Processes and examples in modern and ancient settings: Reviews in Economic Geology, v. 8, p. 261–295.

Pilcher, H., 1965, Acid hyaloclastites: Bulletin of Volcanology, v. 28, p. 283–310.

Poulson, S.R., and Franklin, J.M., 1981, Copper and gold mineralization in an Archean trondhjemitic intrusion, Sturgeon Lake, Ontario: Geological Survey of Canada Paper 81-1A, p. 9–14.

Rittman, A., 1962, Volcanoes and their activity: New York, Wiley, 305 p.

Rogers, N., and van Staal, C.R., 2003, Volcanology and tectonic setting of the northern Bathurst Mining Camp—Part II. Mafic volcanic constraints on back-arc opening, *in* Goodfellow, W.D., McCutcheon, S.R., and Peter, J.M., eds., Massive sulfide deposits of the Bathurst mining camp, New Brunswick, and northern Maine: Economic Geology Monograph 11, p. 181–201.

Rogers, N., van Staal, C.R., McNicoll, V., and Theriault, R., 2003, Volcanology and tectonic setting of the northern Bathurst mining camp—Part I. Extension and rifting of the Popelogan Arc, *in* Goodfellow, W.D., McCutcheon, S.R., and Peter, J.M., eds., Massive sulfide deposits of the Bathurst mining camp, New Brunswick, and northern Maine: Economic Geology Monograph 11, p. 157–179.

Rosa, C.J.P., McPhie, J., Relvas, J.M.R.S., Pereira, Z., Oliveira, T., and Pacheco, N., 2008, Facies analyses and volcanic setting of the giant Neves Corvo massive sulfide deposit, Iberian Pyrite Belt, Portugal: Mineralium Deposita, v. 43, p. 449–466.

Ross, S.L., and Zierenberg, R.A., 1994, Volcanic geomorphology of the SESCA and NESCA sites, Escanaba Trough, *in* Morton, J.L., Zierenberg, R.A., and Reiss, C.A., eds., Geologic, hydrothermal, and biologic studies at Escanaba Trough, Gorda Ridge, offshore northern California: U.S. Geological Survey Bulletin 2022, p. 223–240.

Smith, T.L, and Batiza, R., 1989, New field and laboratory evidence for the origin of hyaloclastite flows on seamount summits: Bulletin of Volcanology, v. 51, p. 96–114.

Soriano, C., and Marti, J., 1999, Facies analysis of volcanosedimentary successions hosting massive sulfide deposits in the Iberian pyrite belt, Spain: Economic Geology and the Bulletin of the Society of Economic Geologists, v. 94, no. 6, p. 867–882.

Sourirajan, S., and Kennedy, G.C., 1962, The system H_2O-NaCl at elevated temperatures and pressures: American Journal of Science, v. 260, p. 115–141.

Sparks, R.S.J., Self, S., and Walker, G.P.L., 1973, Products of ignimbrite eruption: Geology, v. 1, p.115–118.

Sparks, R.S.J., and Huang, T.C., 1980, The volcanological significance of deep-sea ash layers associated with ignimbrites: Geological Magazine, v. 117, p. 425–436.

Stern, R.J., Fouch, M.J., and Klemperer, S.L., 2003, An overview of the Izu-Bonin-Mariana subduction factory, *in* Eiler, J., ed., Inside the subduction factory: American Geophysical Union, Geophysical Monograph Series 138, p. 175–222.

van Staal, C.R., Wilson, R.A., Rogers, N., Fyffe, L.R., Langton, J.P., McCutcheon, S.R., McNicoll, V., and Ravenhurst, C.E., 2003, Geology and tectonic history of the Bathurst supergroup, Bathurst mining camp, and its relationships to coeval rocks in southwestern New Brunswick and adjacent Maine—A synthesis, *in* Goodfellow, W.D., McCutcheon, S.R., and Peter, J.M., eds., Massive sulfide deposits of the Bathurst mining camp, New Brunswick, and northern Maine: Economic Geology Monograph 11, p. 37–60.

von Huene, R., and Scholl, D.W., 1991, Observations at convergent margins concerning sediment subduction, subduction erosion, and the growth of continental crust: Reviews of Geophysics, v. 29, no. 3, p. 279–316.

Walker, G.P.L., 1971, Grain-size characteristics of pyroclastic deposits: Journal of Geology, v. 79, p. 696–714.

Walker, G.P.L., 1989, Gravitational (density) controls on volcanism, magma chamber, and intrusions: Australian Journal of Earth Sciences, v. 36, p. 149–165.

Walker, G.P.L., 1992, Morphometric study of pillow-size spectrum among pillow lavas: Bulletin of Volcanology, v. 54, p. 459–474.

Whalen, J.B., Rogers, N., van Staal, C.R., Longstaffe, F.J., Jenner, G.A., and Winchester, J.A., 1998, Geochemical and isotopic (Nd,O) data from Ordovician felsic plutonic and volcanic rocks of the Miramichi Highlands—Petrogenetic and metallogenic implications for the Bathurst mining camp: Canadian Journal of Earth Sciences, v. 35, p. 237–252.

Wharton, M.R., Hathway, B., and Colley, H., 1994, Volcanism associated with extension in an Oliogocen-Miocene arc, southwestern Viji Levu, Fiji, *in* Smellie, J.L., ed., Volcanism associated with extension at consuming plate margins: Geological Society of London Special Publication 81, p. 95–114.

White, J.D., Smellie, J.L., and Clague, D.A, 2003, Introduction—A deductive outline and topic overview of subaqueous explosive volcanism, *in* White, J., Smellie, J.L., and Clague, D., eds., Explosive subaqueous volcanism: American Geophysical Union, Geophysical Monograph Series 140, p. 1–23.

Whitham, A.G., and Sparks, R.S.J., 1986, Pumice: Bulletin of Volcanology, v. 48, no. 4, p. 209–223.

Wohletz, K.H., 1986, Explosive magma-water interactions—Thermodynamics, explosion mechanisms, and field studies: Bulletin of Volcanology, v. 48, no. 5, p. 245–264.

Wohletz, K.H., and Sheridan, M.F., 1983, Hydrovolcanic explosions—Part II. Evolution of basaltic tuff rings and tuff cones: American Journal of Science, v. 283, no. 5, p. 385–413.

Wohletz, K.H., and Heiken, G., 1992, Volcanology and geothermal energy: Berkeley, California, University of California Press, 432 p.

Yamagishi, H., 1987, Studies on the Neogene subaqueous lavas and hyaloclastites in southwest Hokkaido: Report of the Geological Survey of Hokkaido 59, p. 55–117.

Yamagishi, H., 1991, Morphological features of Miocene submarine coherent lavas from the “Green Tuff” basins—Examples from basaltic and andesitic rocks from the Shimokita Peninsula, northern Japan: Bulletin of Volcanology, v. 53, p. 173–181.

Yamagishi, H., and Dimroth, E., 1985, A comparison of Miocene and Archean rhyolite hyaloclastites—Evidence for a hot and fluid lava: Journal of Volcanology and Geothermal Research, v. 23, p. 337–355.

Yang, K., and Scott, S.D., 1996, Possible contribution of a metal-rich magmatic fluid to a seafloor hydrothermal system: Nature, v. 383, p. 420–423.